A DISSERTATION

ON

"COMBINATORIAL SYNTHESIS OF MAGNETIC HIGH ENTROPY ALLOYS"

Submitted in partial fulfilment of the requirements of the degree of

MASTER OF TECHNOLOGY IN METALLURGICAL AND MATERIALS ENGINEERING

(With specialization in Physical Metallurgy)

Guided By:

Prof. Jochen Schneider

Prof. R. Jayaganthan

Submitted By:

Aparna Saksena

DEPARTMENT OF METALLURGICAL & MATERIALS ENGINEERING

INDIAN INSTITUTE OF TECHNOLOGY, ROORKEE

ROORKEE- 247667 (INDIA)

MAY-2016

CANDIDATE'S DECLARATION

I hereby declare that the proposed work presented in this dissertation titled- "**Combinatorial Synthesis of Magnetic High Entropy Alloys**", in partial fulfillment of the requirements for the award of the degree of **Master of Technology** in **Metallurgical and Materials Engineering** with specialization in Physical Metallurgy, submitted in the **Department of Metallurgy and Materials Engineering, Indian Institute of Technology, Roorkee**, India is an authentic record of my own work carried out during the period from July 2015 to May 2016 under the supervision of **Prof. Dr. R. Jayaganthan**, Professor, Department of Metallurgical and Materials Engineering, Indian Institute of Technology, Roorkee (IIT Roorkee), India and **Prof. Jochen Schneider**, PhD, Professor, Materials Chemistry, Rheinisch - Westfälische Technische Hochschule (RWTH, Aachen), Aachen, Germany.

The matter presented in this dissertation has not been submitted by me for the award of any other degree.

Dated:

Place: Roorkee **APARNA SAKSENA**

CERTIFICATE

This is to certify that the above statement made by the candidate (Aparna Saksena) is correct to the best of my knowledge and belief.

Dr. R. Jayaganthan
Professor
Department of Metallurgical and
Materials Engineering
Indian Institute of Technology, Roorkee
Roorkee–247667, (India)

Dr. Jochen Schneider
Professor
Materials Chemistry
RWTH, Aachen
Aachen-52074, (Germany)

ACKNOWLEDGEMENT

During the whole journey from the discussion of the Project title to the submission of this thesis, there are many individuals that I would like to thank and hence I will now take the opportunity to express my gratitude to Dr. R. Jayaganthan, Professor, Department of Metallurgical and Materials Engineering, IIT Roorkee and Prof. Jochen Schneider, PhD, Materials Chemistry, RWTH Aachen, for giving me this opportunity to work on such a new and unexplored topic and for putting their faith in me. I am also very grateful to Dr. K.G. Pradeep, Atom Probe Group Leader at Materials Chemistry, RWTH Aachen, for his expert and kind guidance towards my thesis work. My work would have been directionless without their encouragement, constant and patient guidance.

I am very grateful to our respected Head of Department Prof. S.K. Nath for providing all the facilities required to carry out the work.

I am also very thankful to Mr. Marshal Amalraj for his scientific help, inspiration and valuable suggestion throughout the experimentation. In this regard, I would also like to thank both Dr. Denis Music and Mr. Marshal Amalraj for their contributions towards the theoretical simulations used in the thesis.

I would like to thank Mr. Oliver Hunold, Mr. Jan Ole Achenbach, Ms. Friederike Wittmers, Mr. Holger Rueß and Mr. Marcus Hans for their indispensable help and guidance in operating different equipment.

I would also acknowledge the valuable contributions from the technical staff at Materials Chemistry, RWTH Aachen and Metallurgical and Materials Engineering Department, IIT Roorkee for helping me access the labs and equipment, taking care of the safety of every individual.

I am also greatly indebted to Deutscher Akademischer Austausch Dienst (DAAD) and MHRD, Govt. of India. Without their generous funding and support, the project would have not been possible.

Last but not the least, I would like to thank my Family and Friends for their constant moral support during the project work.

ABSTRACT

High Entropy Alloys are a new class of alloys that have gained a lot of interest because of their outstanding mechanical properties even at low temperatures. Present study focuses on designing a HEA having notable magnetic properties. Due to the presence of multiple components in the system, prediction of the number of phases and their type is difficult considering the limitations in empirical or thermodynamic predictions.

To study the effect of each constituting element, a 5 component system comprising of Fe, Mn, Ni, Co, Nb as constituent elements if investigated starting from binaries, ternaries until quaternary and quinary systems. Such a detailed investigation allows for the identification of regions exhibiting single phase solid solution over a wide compositional space. Thin films of these systems are sputtered using custom designed physical vapor deposition system, exploiting the advantages of Combinatorics. Using inferences from these systems a single phase BCC FeMnNiCoNb (varying Nb content from 5at% to 9 at%) alloy system was obtained which exhibited ferromagnetic behaviour.

LIST OF CONTENTS

LIST OF FIGURES

LIST OF TABLES

LIST OF SYMBOLS

HEA- High Entropy Alloys

ΔG_{mix} – Gibb's Free Energy of Mixing

ΔH_{mix} – Enthalpy of Mixing

T – Temperature

ΔS_{mix} – Entropy of Mixing

c_i - Atomic fraction of i^{th} element

r_i – Atomic radius of the i^{th} element

ΔH^{AB}_{mix}- Enthalpy of mixing of A and B elements

CHAPTER 1

INTRODUCTION

Conventionally, metallic alloys are known to have one or two major constituting elements. One element, primarily being the principle element is considered as the solvent. Some more constituents in small proportions are added, to achieve the final desired properties. [1]

However, High Entropy Alloys are defined to have five or more principle constituting elements, each having chemical composition ranging from 5 to 35 atomic percent. There exists no distinguishable solvent or solute element. This concept is utilized to design advanced materials that show unique properties which cannot be attained by conventional micro alloying.[2] They are associated with high lattice distortion because of the presence of different neighboring atoms with different atomic radii, throughout the lattice. They are expected to possess high solid solution strengthening and excellent resistance against high temperature softening.[3]

As the name suggest, the design strategy was initially based on the thermodynamic considerations to increase the configurational entropy of the system, by increasing the number of components and their concentration close to equiatomic concentration. This concept of maximizing the configurational entropy is expected to form a thermodynamically stable single phase solid solution instead of multi phased structure or intermetallics (explained in detail, later in the following sections). However, predicting the crystal structure and no. of phases formed in these alloys, is still a challenge. Also, each component of the system has its unique role in stabilizing a particular phase or numerous phases. Changing the concentration of any of the component can alter not only the properties of the system but also the phase formed.

These alloys have gained popularity and are studied considerably in the recent times. Many experiments are conducted and documented on the phase prediction and mechanical properties of these alloys. Various alloy systems have been investigated to have high tensile strength, ductility and high temperature stability [3-5]. These alloys can be probed in terms of their functional properties such as magnetism , as these alloys consists of 5 or more elements and if selected prudently, these elements can enhance the magnetic properties significantly via

induced exchange coupling among the different atoms. Certain high entropy alloy systems are reported to have exhibited magnetic properties. However the efforts directed towards magnetic property exploration are not that significant.

Present study aims at exploring the magnetic Properties of such an alloy system via combinatorial alloy design. Combinatorial method will expedite the study, while the effect of each element in the system and their effect on magnetic property variation could be investigated. Also effect of each element in phase formation is studied in detail.

CHAPTER 2

LITERATURE REVIEW

2.1. THERMODYNAMICS OF HIGH ENTROPY ALLOYS

The initial conviction behind the design of these alloys is maximization of the configurational entropy that can aid in stabilizing simple solid solution based alloys.

Thermodynamically, a system can be stabilized by increasing the negative Gibb's Free Energy of that system. According to the following equation, …[6]

$$\Delta Gmix = \Delta Hmix - T\Delta Smix$$

For a negative ΔHmix of the components, increasing the configurational entropy (ΔSmix has major contributions from both thermal entropy and configurational entropy. If the change in volume or heat is zero then simply configurational entropy can be taken into consideration [6]) can decrease the Gibb's Free Energy and thus can stabilize simple solid solution for a 5 (or more) component system rather than forming ordered intermetallics.

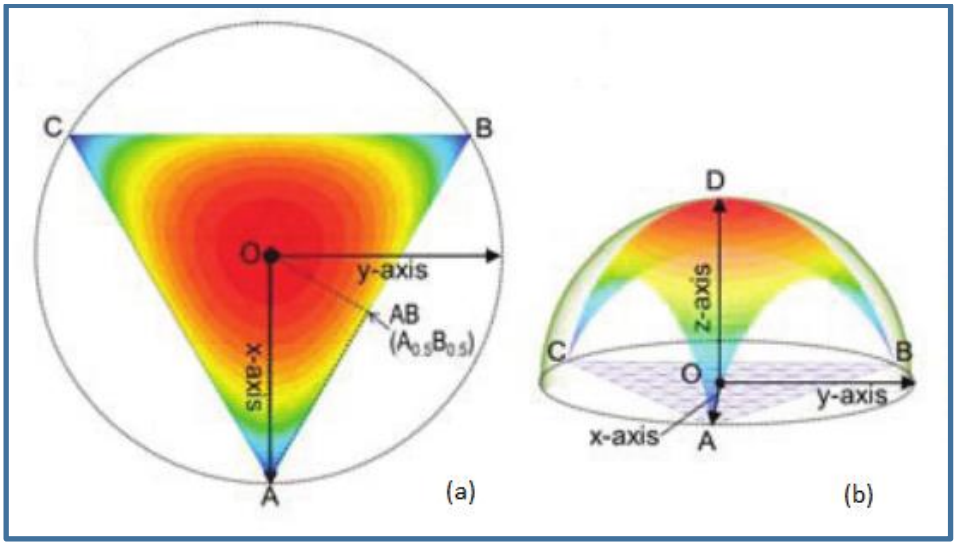

Figure 2-a Composition Configurational Entropy diagram (C-CE) for an A-B-C Ternary System, showing maxima of Configurational Entropy at the Equiatomic concentration[7]

Figure 2-a-shows maxima of configurational entropy at or near Equiatomic composition for a Ternary system. This increase in configurational entropy can also be attributed from the equation below

$$S = k\, ln\omega$$

Where ω can be defined as the no. of discrete ways in which the atoms can be arranged in a system. Increasing the no. of components and their atomic concentrations close to equiatomic concentration, will increase ω and thus increase the configurational entropy, decreasing ΔGmix hence, expected in stabilizing random solid solutions.

However, experimentally achieving a single phase in these alloys is complicated and role of Configurational Entropy is still in debate. There are certain design criteria that can predict the phase formation in HEA, but to a limited extent. [1, 4]

2.2. DESIGN CRITERIA FOR HEA

Single phase solid solution formation in HEA looks obvious from the thermodynamic perspective. Despite of the thermodynamic agreement, there are some other considerations that are required to be followed in order to achieve a single phase solid solution.

2.2.1. ATOMIC SIZE DIFFERENCE

According to Hume Rothery Rule, there are 4 factors that govern formation of single phase solid solution-Atomic size difference, Electro Negativity difference between the constituting elements, crystal structure and valence electron concentration. Similar to the conventional metallic alloys, this parametric variation (Atomic Size Difference) in case of HEA can be defined as follows:[8]

$$\delta = \sqrt{\sum_{i=1}^{N} c_i \left(1 - r_i / \left(\sum_{i=1}^{N} c_i r_i\right)\right)^2}$$

2.2.2. ENTHALPY OF MIXING

Similarly Enthalpy of mixing can be given by the following relation[8]

$$\Delta Hmix = \sum_{i=1, i\neq j}^{N} 4\Delta H_{mix}^{AB} c_i c_j$$

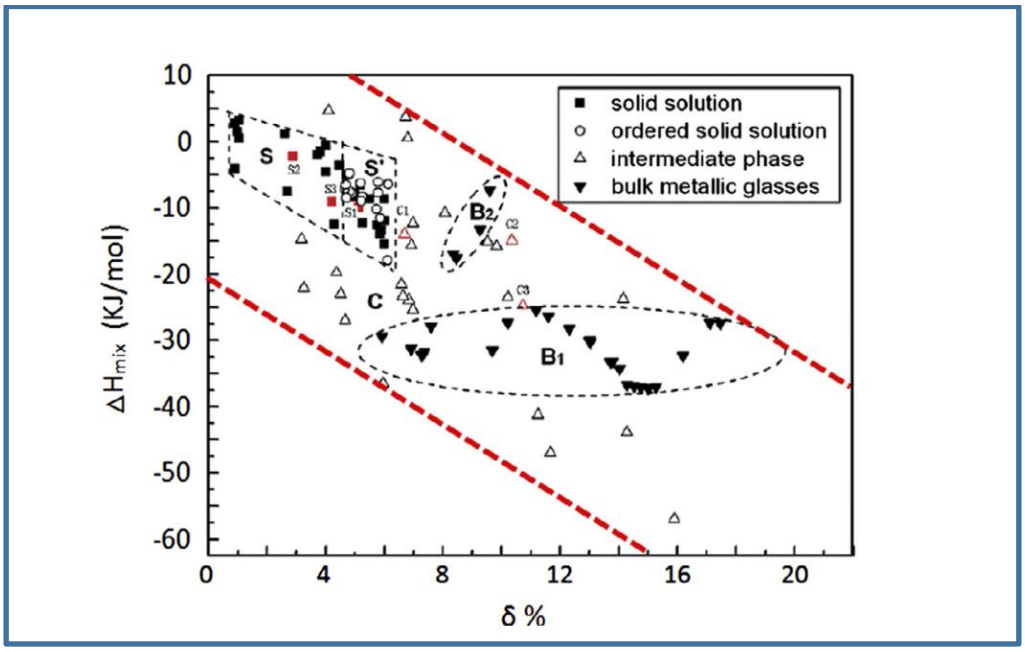

Figure 2-b - A map between Enthalpy of Mixing, $\Delta H_{AB}^{(mix)}$ and Atomic Size difference, δ, predicting the phase formation. Random Solid Solution is favored for $-10KJ \leq \Delta H_{mix} \leq 5KJ$ and $\delta \leq 5\%$. Region for $-20KJ \leq \Delta H_{AB}^{(mix)} \leq 0KJ$ and $5 \leq \delta \leq 6.6\%$ shows a transition from random solid solution to ordered solid solution.[8]

The conditions defined for the formation of a single phase random solid solution can therefore be given as: (according to Zhang et al [8])

$$\mathbf{-10KJ \leq \Delta H_{mix} \leq 5KJ \text{ and } \delta \leq 5\% \text{ and } \Delta S_{mix} \geq 13{,}38J/K\ mol}$$

2.2.3. VALENCE ELECTRON CONCENTRATION

This concept also predicts the formation of a FCC or BCC phase on the basis of the valence electron concentration which can be calculated by the following expression.[9]

$$VEC = \sum_{i=1}^{N} c_i\,(VEC_i)$$

FCC phase is stable for VEC ≥ 8 whereas BCC is said to be stable for VEC ≤ 6.4, where VEC_i represents Valence Electron Concentration of i^{th} element.

Although these criteria does not effectively predict the formation of random solid solution or intermetallics but provide an approximate idea on solid solution formation in HEAs on the basis of the fundamental characteristics of the elements constituting the alloy.[9]

2.2.4. THEORITICAL SIMULATIONS

There are various simulation techniques that have been employed to envisage the phase formation in these alloys such as DFT Calculations, ab Initio molecular dynamic simulations, CALPHAD and many others.

One can keep following points in mind before designing an alloy of the required properties.

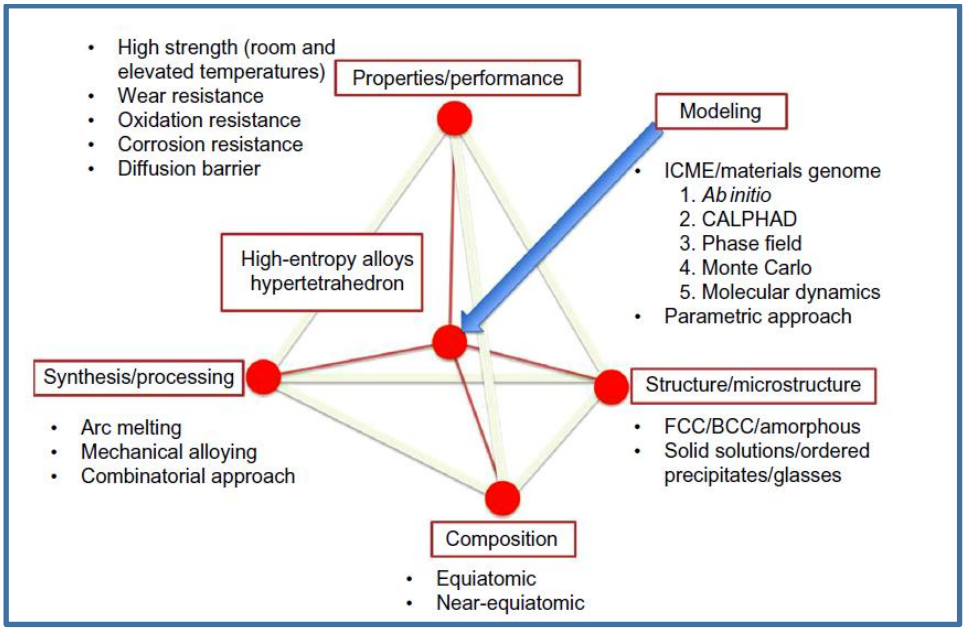

Figure 2-c Material Hyper Tetrahedron for HEA [10]

2.3. CHARACTERISTIC FOUR CORE EFFECT IN HEA

2.3.1. HIGH ENTROPY EFFECT

According to Gibb's Phase rule, no. of phases (P) that can be present at constant pressure can be given by the following equation

$$P = C + 1 - F$$

Where C is the no. of Components in the system and F represents the thermodynamic degrees of freedom. For a five component system, one can expect a maximum of six phases but however in HEA, it is expected that a single solid solution phase forms instead of intermetallics. Also the no. of multiple phase formation reported in HEAs is much lesser than that predicted by the phase rule. It can be said that the high entropy of these alloys can extend the solubility of the constituting elements in one another. [11]

2.3.2. SLUGGISH DIFFUSION EFFECT

In comparison to the conventional alloys, these alloys have much lower diffusion coefficient as long-range diffusion requires cooperative movement of atoms. In case of HEAs, atoms surrounding a particular vacancy competes differently because of the difference in chemical identity. It can be ascribed to a larger fluctuation of lattice potential energy between lattice sites, as proposed.

This effect can influence the growth characteristics, morphology and distribution of the new phase etc. [2, 11]

2.3.3. SEVERE LATTICE DISTORTION EFFECT

Being a multicomponent system, every atom is surrounded by different atoms. The matrix undergoes lattice strain because of the atomic size difference associated with every component present in the system. Other factors like different bond energy, different neighboring atoms and also different electronic structure can lead to these lattice strains, resulting in high lattice distortion.

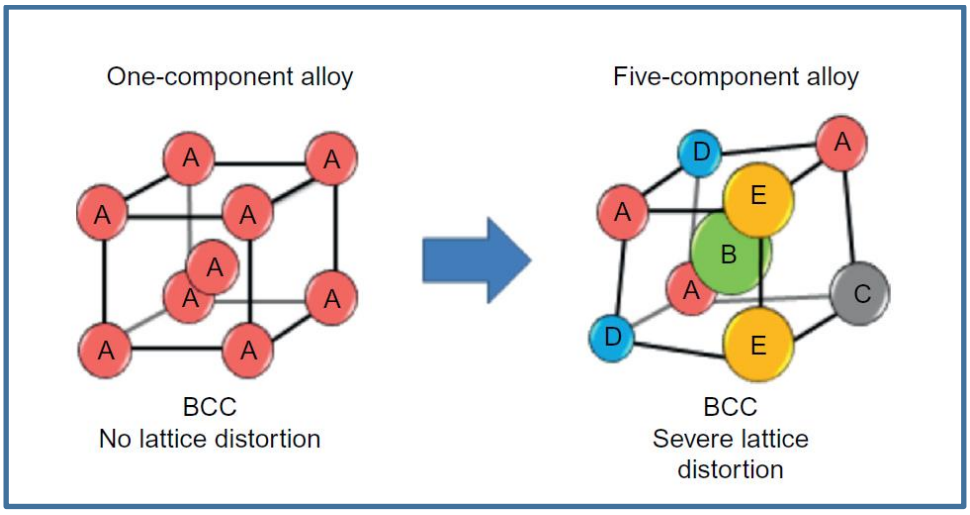

Figure 2-d A schematic diagram to represent Lattice distortion in case of 5 component system [11]

2.3.4. COCKTAIL EFFECT

The phases present in the system can be one or more but the property contribution is from all the components of the system and varying the composition can greatly alter the properties of the alloy.

2.4. MAGNETIC PROPERTIES INVESTIGATED IN THE PAST

Very few studies have been conducted when it comes to the Magnetic characterization of these alloys. Here are some discussed very briefly:

Kao et al. have investigated the electrical and magnetic properties of $Al_xCoCrFeNi$ system in homogenized conditions at different temperatures (5K, 50K and 300K). The alloy was produced by vacuum arc re-melting. Al content is varied and therefore the crystal structure. It was observed that at low temperature, a BCC phase has a higher saturation magnetization than a FCC phase. Also on increasing the Al content, saturation magnetization of both BCC and FCC phase was seen to decrease because of the formation of AlNi-rich phase which is Ferro-magnetically weak.[12]

Liu et al. investigated the microstructure and magnetic properties of $FeNiCuMnTiSn_x$ system (x=0, 0.05, 0.1, 0.5 and 1). The alloy was prepared by arc furnace. The microstructure was seen to change on increasing the Sn content, from mixed intermetallic to a single phase structure. The Saturation Magnetization value is found to increase gradually from 0.34 to 15.8 emu/gm on increasing the Sn Content (ref Table 2-1). On increasing the Sn content, magnetic transformation is observed from paramagnetism to super paramagnetism to a soft ferromagnetic behavior at X=1.[13]

Alloy	Saturation Intensity (emu/gm)	Remanent Magnetism (emu/gm)	Coercive Force (Oe)
FeNiCuMnTi	0.34	0.001	310.45
FeNiCuMnTiSn(0,05)	0.36	0.002	306.31
FeNiCuMnTiSn(0,1)	0.37	0.001	155.89
FeNiCuMnTiSn(0,5)	4.42	0.061	60.92
FeNiCuMnTiSn(1)	15.81	0.277	71.27

Table 2-1Magnetic Properties of $FeNiCuMnTiSn_x$ [13]

Lucas et al. studied $FeCoCr_xNi$ system which exhibits a single phase FCC structure, prepared by arc melting. Equiatomic FeCoNiCr is ferromagnetic at 130K and on decreasing the Cr content this Curie temperature is seen to be increasing. Cr is antiferromagnetic and therefore its net effect is to cancel/decrease the moment of the ferromagnetic elements[14]. Another experiment documented by Lucas et al. studies the effect of adding Palladium to the above mentioned system. The alloys are prepared by arc melting and then the as-cast samples are rolled to a desired dimension. Addition of Pd in FeCoNiCr (which is paramagnetic at RT) increases the lattice parameter of the FCC lattice and also increases the saturation

magnetization values at room temperature of the system as a whole. However the magnetization value is still much lower than that of pure Fe (ref Table 2-2). This study also focused on the variation of magnetic moments of these alloys (along with $FeCoCrNiAl_2$, ordered BCC lattice and FeCoCrNiAlCu, 80% phase fraction of FCC+BCC lattice) with temperature[15]. Curie temperature and saturation magnetization value of FCC transition metal alloys are predicted by Körmann et al. Computational methods are used on FeCoNiCrPd alloys. Theoretical results are in quite good agreement with the experimental data. They also suggested Ag, Au and Cu as alternative to Pd alloying that can exhibit room temperature ferromagnetism [16].

High Entropy Alloys studied	Saturation magnetization	Phases Formed	Curie Temperature	$(k_b/atom)S^{rss}_{conf}$
	emu/g, Am^2/Kg at RT		°C	
FeCoCrNiAlCu	41 (16)	FCC+BCC	-	1.792
FeCoCrNiAl2	13 (18)	BCC	157 (268)	1.561
FeCoCrNiPd2	34	FCC	230	1.561
FeCoCrNiPd	33	FCC	167	1.609
FeCoCrNi	3	FCC	Paramagnetic	1.386
FeNi	129	FCC	517	0.693
Fe	218	BCC	773	0
Co	143	HCP	1115	0
Ni	48.5	FCC	354	0

Table 2-2Magnetic Properties studied by Lucas et. al. [15]

Ma et al studied the effect of Nb content on the microstructural and the magnetic properties of $AlCoCrFeNb_xNi$. The alloy prepared by arc melting showed 2 phases- BCC + Laves phase (CoCr) Nb type. However, $AlCoCrFeNb_{0.1}Ni$ is a single BCC solid solution phase with the maximum residual magnetization (in this HEA family) of 6,016 emu/gm. Coercivity increases with addition of Nb.[17]

High Entropy Alloys studied	Saturation magnetization	Phases Formed
	emu/g, Am^2/Kg	
AlCoCrFeNiNb	10.31	Laves+(Laves+BCC)
$AlCoCrFeNiNb_{0.75}$	17.61	BCC+ (Laves+BCC)
$AlCoCrFeNiNb_{0.25}$	34.69	BCC+ (Laves+BCC)
$AlCoCrFeNiNb_{0.1}$	49.56	BCC
AlCoCrFeNi	64.71	BCC

Table 2-3 Magnetic Properties of AlCoCrFeNiNb. [17]

The ferromagnetic behavior of AlCoCrCuFeNi system is studied by Singh et al. It is ascribed to the decomposition of FeCoCr rich region into FeCo rich and Cr rich domains. The alloy is prepared by melting the constituents in an induction levitation furnace and casted, also splats are produced and then aged. The aged alloy shows a higher saturation value when compared to the as cast alloy (ref- Table 2-4). Zhang et al investigated the magnetic properties of this alloys system and showed that ageing this alloy at 1000°C decreases the magnetization saturation from 38emu/gm to 16 emu/gm [18]. This has been argued by Singh et al by explaining that aging of FeCoCr alloys in the region of miscibility gap improves the ferromagnetic properties as it broadens the spinodal region and therefore this finding is not unanticipated as aging at 1000°C does not correspond to this region.[19]

Materials	Ms at 1.5T, 320K	Coercivity at 320K	Ms at 14T, 300K
AlCoCrCuFeNi	emu/gm	Oe	emu/gm
Splat quenched	41	11±10	46
As- cast	36	44±10	44
Aged	40	264±10	48

Table 2-4 Magnetic Properties of AlCoCrCuFeNi. [19]

Wang et al have contributed in the investigations of the Magnetic properties of CrFeCoNiCu and AlCrFeCoNiCu alloy system. The former alloy system is seen to be paramagnetic, however addition of Al results in phase decomposition into NiAl intermetallic and α-Fe,Cr solid solution, favoring the ferromagnetic behavior with saturation value of approximately 40 emu/gm [20].

$CoCuCrFeNiTi_x$ (FCC to FCC+ laves phase) and 6(Fe)NiCoCrAlTiSi systems are studied by Wang et al and Zhang et al respectively [21, 22]. However the former shows a transition from paramagnetism to super paramagnetism on increasing Ti content, the latter alloy shows a soft magnetic behavior with a saturation magnetization value of 20.04 emu/gm, attributed to an increase in Fe content.

There are some other recorded efforts that investigated this functional property in HEA [23-27]. In spite of these efforts, all these alloy systems fail to show magnetic properties comparable to the conventional ferromagnetic elements (Fe, Co and Ni). However, they assert the fact that if the constituents, composition and structure are tailored vigilantly, these alloys can prove themselves to be a potential magnetic alloy.

CHAPTER 3

MATERIAL SELECTION

The aim is to design a High Entropy Alloy showing superior magnetic properties, as discussed previously. On the basis of literature studied so far, certain properties are desired.

- A combination of transition metals that together show superior magnetic properties, forming a HEA.
- Most of all, a single phase, disordered BCC structure is desired.. Magnetic properties related to multi-phase are generally non reproducible. Therefore, stable single phase provides an ideal base for the structure sensitive properties specially coercivity and permeability.[28]

In this regard, FeMnNiCoNb Alloy system is scrutinized in the present study.

- Fe, Ni and Co are ferromagnetic in nature.
- Mn induces ferromagnetic spin coupling. As in the case of Heusler alloys Mn is known to induce magnetic moments in a lattice containing nonmagnetic elements. Its net effect is to increase the average magnetic moment of the alloy system.
- Nb is added to stabilize a BCC Structure.

Some fundamental properties of these elements are listed below

The ΔH_{AB}^{mix} for the element combination is given in the Table 3-1.

Mn	0	-5	-8	-4
0	Fe	-1	-2	-16
-5	-1	Co	0	-25
-8	-2	0	Ni	-30
-4	-16	-25	-30	Nb

Table 3-1 The Values of $\Delta H_{AB}^{(mix)}$ (KJ/mol) calculated by Miedema's Model for Atomic Pair between the Elements Chosen[29]

As one can see from the table of ΔH_{AB}^{mix}, Nb has a very high negative Enthalpy of mixing with all the other elements. Also from Table 3-2 Nb has a higher atomic radius in comparison to

the other elements in the alloy system. Hence it is necessary to study the effect of varying Nb content in the alloy system.

Elements	Atomic Radius (nm)[2]	Valence Electron Concentration[9]	Electro negativity[30]	Crystal Structure
Mn	0.135	7	1.55	α-Mn
Fe	0.12412	8	1.83	BCC
Co	0.1251	9	1.88	HCP
Ni	0.12459	10	1.91	FCC
Nb	0.1429	5	1.6	BCC

Table 3-2 Fundamental properties of the elements.

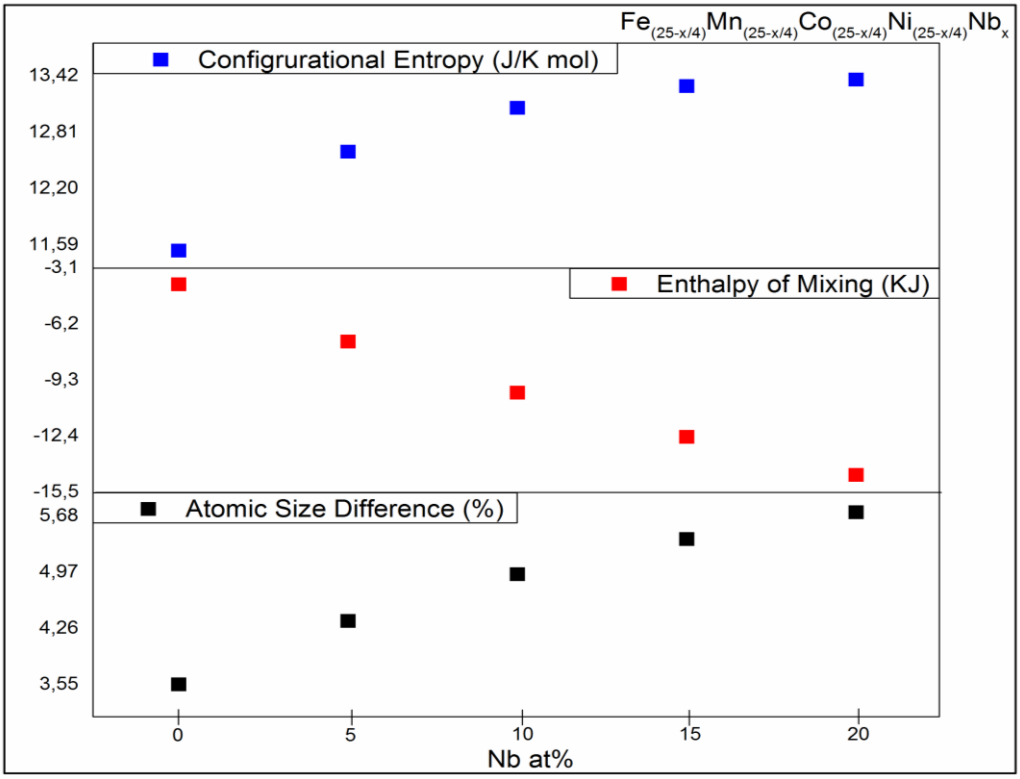

Figure 3-a Parametric calculations on the FeMnNiCoNb alloy system, using the formulas discussed in the previous section.

Some basic calculations by varying the Nb content in the FeMnCoNi quaternary alloy system are (discussed in the previous section) performed and are shown as follows:

On increasing the Nb content, as one can see from Figure 3-a, that with an increase in the configurational entropy, there is a simultaneous increase in atomic size difference and negative enthalpy of mixing. Hence one can decipher from the graph that selection of an optimum Nb content can favor the formation of a simple solid solution single phase.

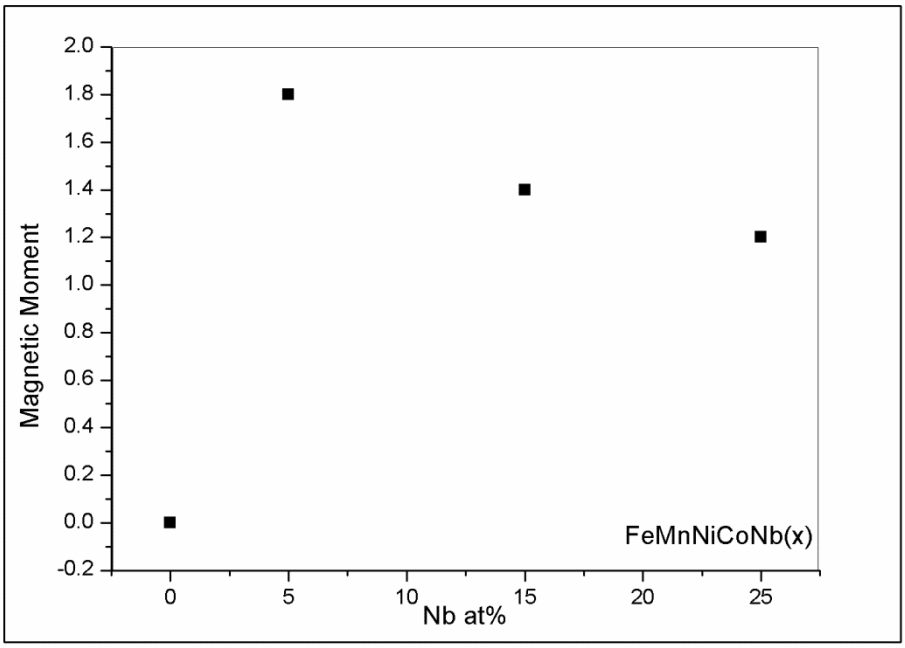

Figure 3-b Ab-Initio calculation showing change in magnetic moment with variation in Nb content.

Ab initio calculations are performed to analyze the possible stable phase and the observed magnetic moments for the alloy system, varying the Nb content is represented in Figure 3-b. The magnetic moments of an FCC structure is assumed to be 0 in comparison to a BCC structure. As shown, maximum magnetic moments are observed for a BCC containing 5 at% Nb.

CHAPTER 4

EXPERIMENTATION

The elements (Fe, Mn, Ni, Co and Nb) selected are used in the form of a 12.7cm Ø (2”) targets 99.95% purity, in an Ultra High Vacuum Magnetron sputtering chamber. Since the chamber has provision to sputter simultaneously from only 4 targets, to sputter the 5 component system Fe/Mn Alloy , Pure Ni, Pure Co and pure Nb are used as the 4 targets. The Substrates used for deposition are Si and Sapphire Substrates (2 inches in diameter)

4.1. UHV MAGNETRON SPUTTERING

Sputtering is carried out in a custom designed PVD system, at Materials Chemistry, RWTH Aachen. The system provides an advantage to sputter from four targets, simultaneously, thus producing multiple compositions on a single sample. The system is HPPMS (High Power Pulse Magnetron Sputtering) compatible with a possibility of substrate bias also. However, for the present study, the system is run in DC mode. Additional standard equipment used during the study are:

- MELEC Pulse Generator
- Surface sample holder/ heater.

Figure 4-a shows the actual system installed in MCh RWTH Aachen.

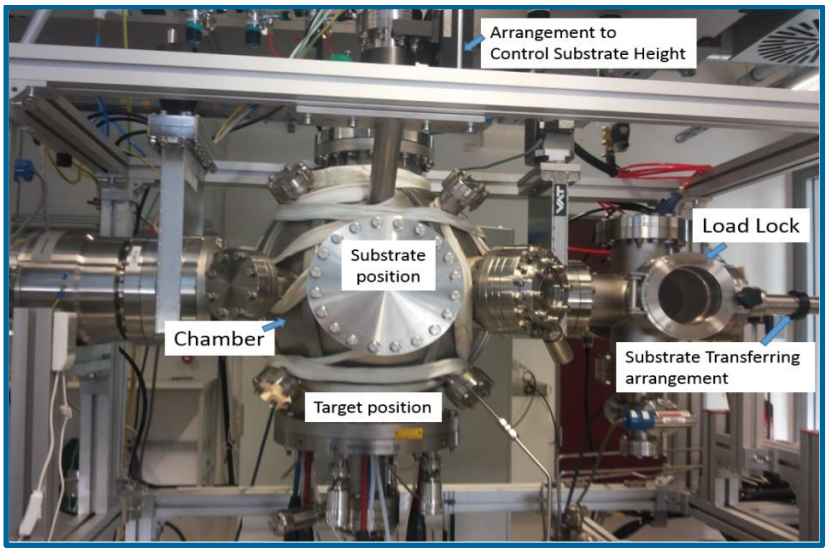

Figure 4-a Kybele setup at Materials Chemistry, RWTH Aachen

Figure 4-b (i) shows a schematic representation of the positioning of targets and the substrate inside the chamber used. Figure 4-b (ii) (inset) shows a schematic of an ideal combinatorial sample after being sputtered. Chemical gradient is likely to be observed during characterization.

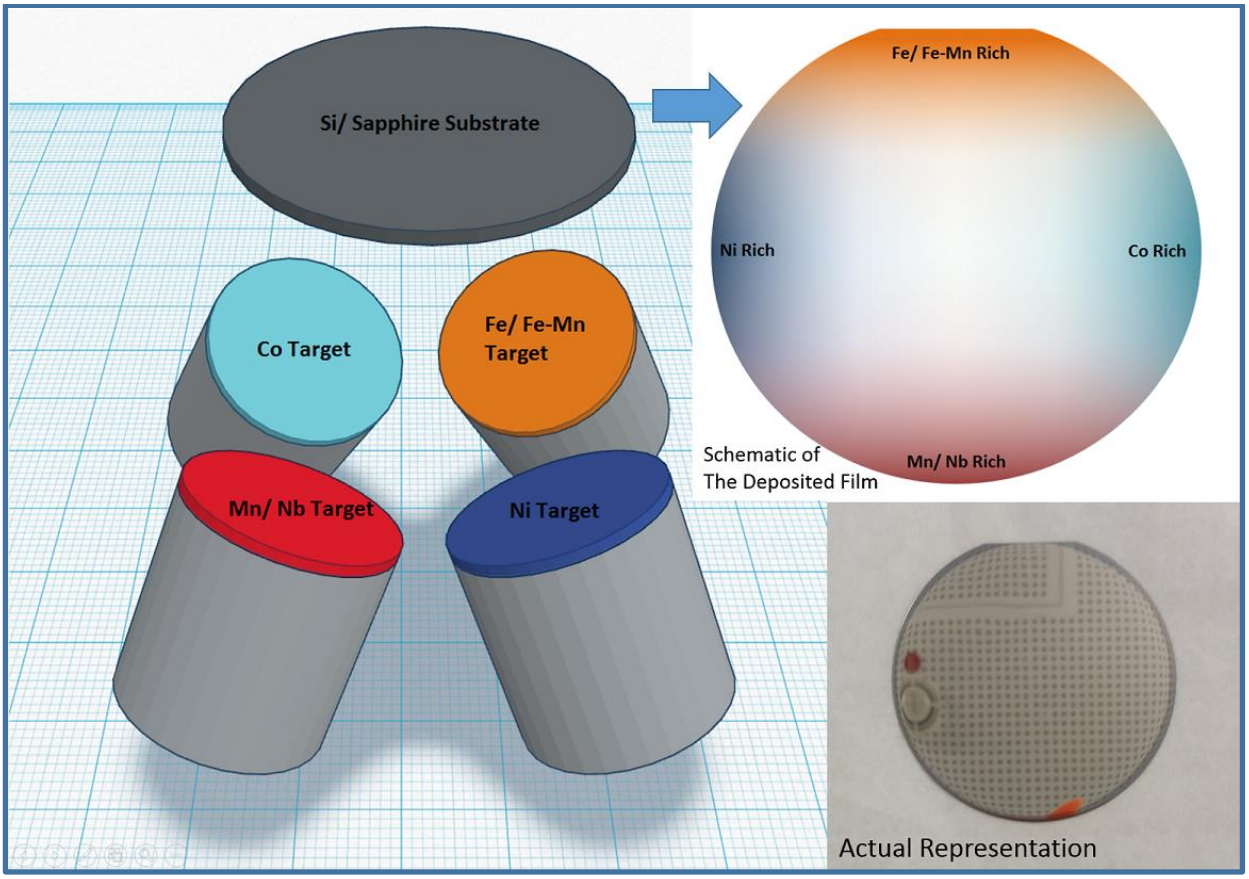

Figure 4-b Schematic of the arrangement inside the sputtering chamber and the combinatorics sample after sputtering.

The chamber pressure before and after sputtering is maintained to be around 10^{-7} to 10^{-8} Torr. During sputtering Argon is used as the base gas in the chamber, purged for 10 minutes before the start of sputtering. The chamber pressure during sputtering is maintained at 3.03 $x10^{-3}$ Torr.

Substrate heating is carried out in certain cases. Overall sputtering temperature is varied for different samples, from Room Temperature to 300℃ (increasing 10℃/min). The substrates are deposited with the target material from 25 to 45 minutes depending on the no. of targets used. The thin film of approximately 1μm thickness is deposited. During sputtering, various targets are employed with different voltages to obtain a different compositional contribution from each element.

4.2. ENERGY DISPERSIVE X-RAY SPECTROSCOPY

EDX is carried out on JEOL JSM-6480 Scanning Electron Microscope. It has a Tungsten Filament as the Thermionic Emitter. Acceleration voltages from 2KV to 30 KV can be used. This system is equipped with EDAX Genesis 2000 software which contains 3 main components, an X-Ray detector, separated from the SEM chamber by a thin polymer window; a pulse processing circuitry which determines the energy of the characteristic x-rays emitted and an analyzer equipment to interpret the x-ray data and communicate it to the computer screen. Figure 4-c shows the electron microscope installed at MCh RWTH Aachen.

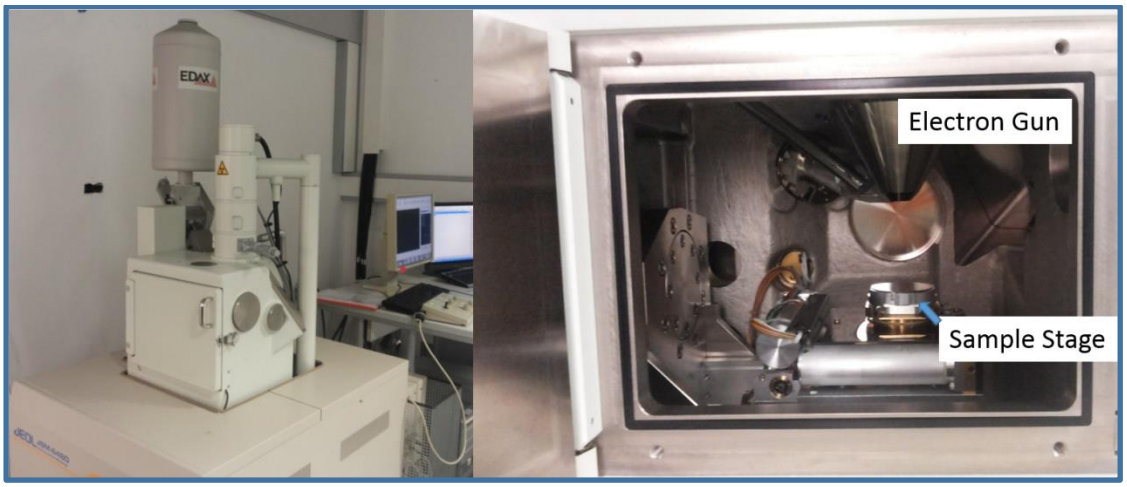

Figure 4-c SEM installed at Materials Chemistry, RWTH Aachen.

In the present study, all the samples are measured with an acceleration voltage of 15KV at a working distance of 10mm, magnified by 1500X for 100 seconds. EDX is measured on the spots as shown in the Figure 4-d, to analyze the gradient in composition as a result of the combinatorics arrangement in the sputtering chamber.

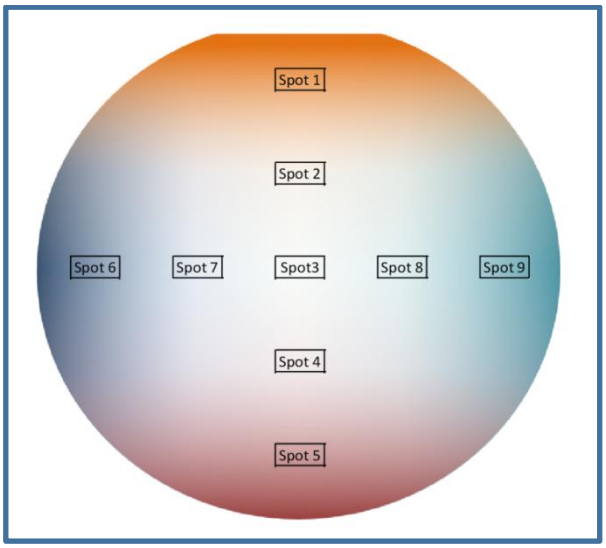

Figure 4-d Schematic of the combinatorics sample sputtered, representing the spots on which the measurement is done.

4.3. X-RAY DIFFRACTION

XRD patterns are measured on the sputtered thin films with the help of Bruker axs D8-discover, General Area Detection Diffraction System. The instrument is designed to measure at a grazing incidence angle, especially to measure thin films. This arrangement helps in restricting diffraction only from the film, avoiding deeper penetration of x-rays that can give information from the substrate. Figure 4-e shows the instrument on which all the measurements are taken.

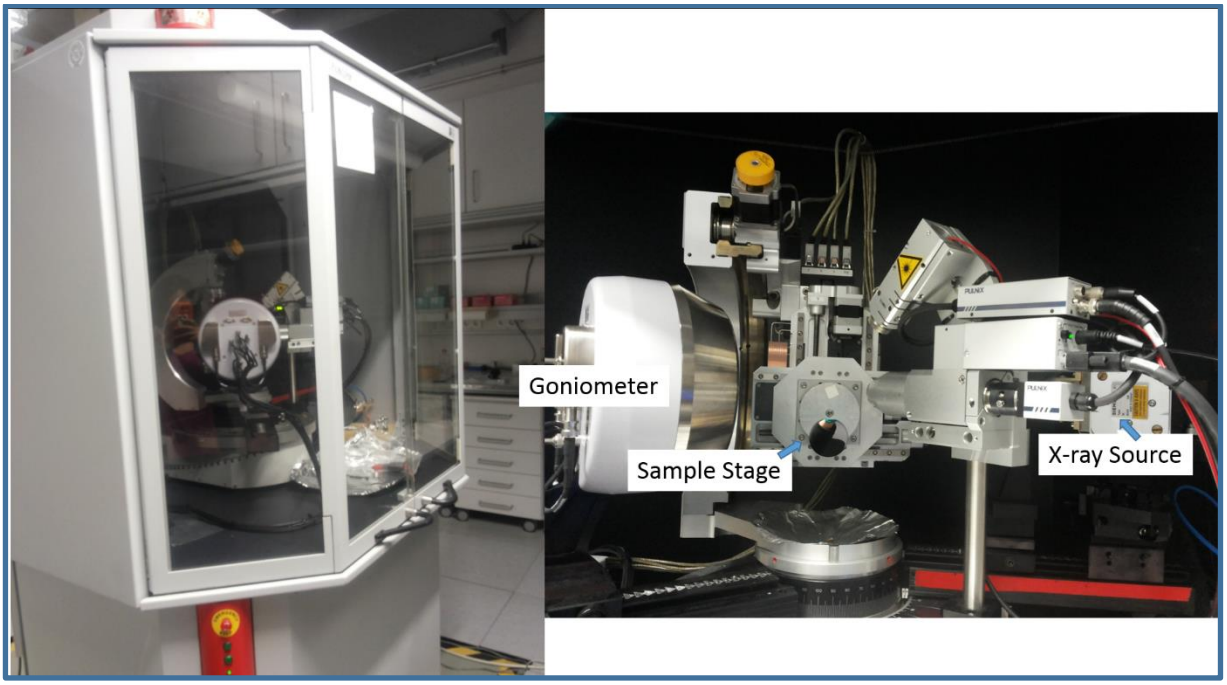

Figure 4-e X-Ray Diffractometer installed at Materials Chemistry, RWTH Aachen.

The spot size was 1x3 mm^2 for the incidence angle ≥10˚. For the present study, the instrument is used to do a 2-θ scan of the samples sputtered to analyze the phases formed for the particular composition (measured via EDAX, mentioned above). Co (λ = 1.789 Å) x-ray source is used to measure all the diffraction patterns. The angle of incidence used is 10°.

4.4. NANO INDENTATION

Nano Indentation is performed on Hysitron TI-950 Indenter (Figure 4-f) with a diamond tip of Berkovich geometry. The goal is to obtain Elastic Modulus and Hardness values for different compositions sputtered, by the help of load displacement curves

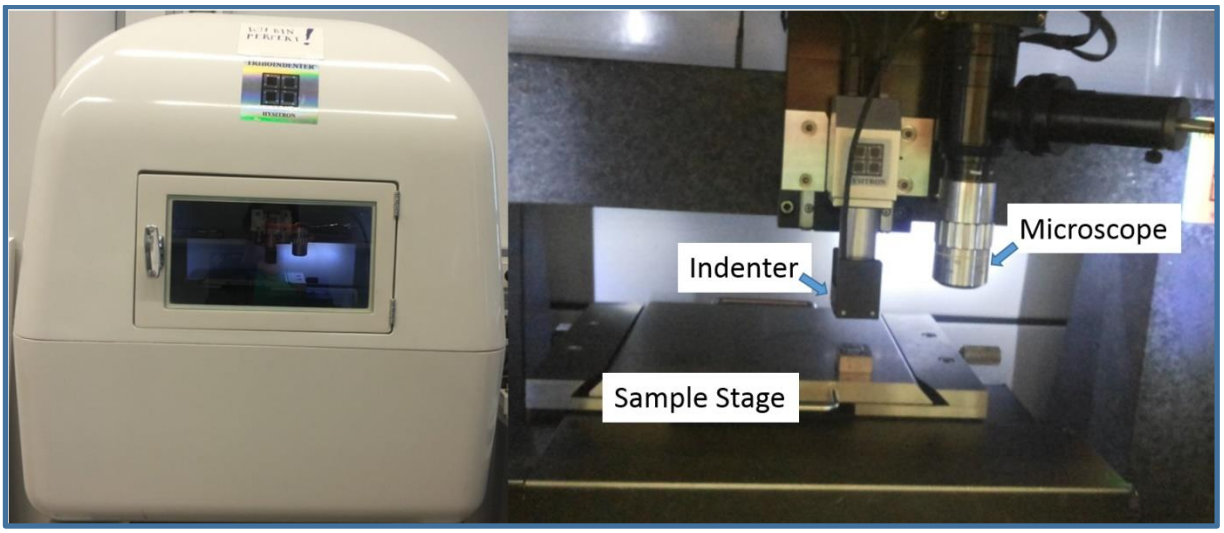

Figure 4-f Nano Indenter installed at Materials Chemistry, RWTH Aachen

For the present study the maximum load applied was 2000 μN and a minimum of nine indents are taken for the same composition to get a precise Hardness and Elastic Modulus value.

4.5. ATOM PROBE TOMOGRAPHY

A 3-D LEAP 4000X HR from CAMECA (Figure 4-g) is used to analyze the elemental distribution on a Nano scale. The samples are prepared using a FEI Helios Nanolab 660 focused ion beam.

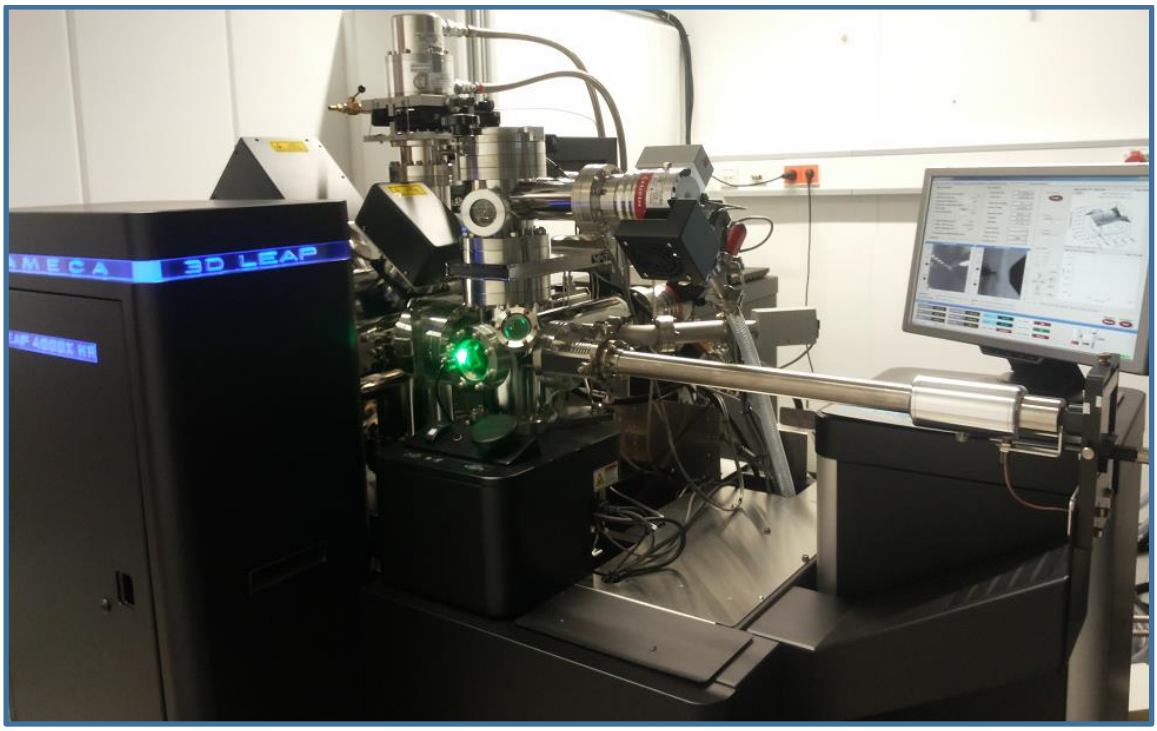

Figure 4-g 3-D LEAP installed at Materials Chemistry, RWTH Aachen.

4.6. TRANSMISSION ELECTRON MICROSCOPY

Transmission Electron Microscopy was performed in a TITAN 60-300 microscope operated at 300 kV situated at Forschungszentrum, Jülich.

4.7. MAGNETOMETRY

The magnetic property analysis of various representative samples are done on a Vibrating Sample Magnetometer (VSM), Model 600 Physical Property Measurement System at Jülich Center for Neutron Research (JCNS), Jülich Forschungszentrum.

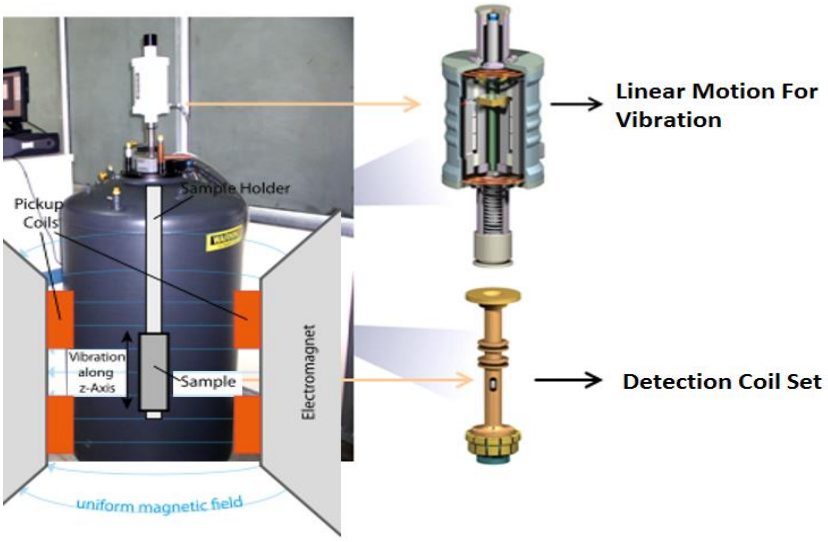

Figure 4-h A schematic of VSM showing the sample placement and the mechanism of the instrument briefly.[31]

A vibrating sample magnetometer (Figure 4-h) is used to measure the magnetic moments of the sample, placed inside it. This requires the sample to be kept in uniform magnetic field which magnetizes it, inducing magnetic moments. This sample is then physically vibrated, sinusoidally. Therefore there is a change in magnetic flux which results in an induced voltage in the sensing coils, placed nearby, i.e. is proportional to the magnetic moments of the sample. [32]

For the present study, samples are magnetized at a magnetization field of 3 to 6 Tesla. The film is cut into an approximate dimension of 3x4mm with the help of a diamond cutter and is mounted with the help of a diamagnetic glue on the holder with the substrate (also the substrate is diamagnetic) itself. The system is ideal for measuring the magnetic properties of a thin film.

CHAPTER 5

RESULTS AND DISCUSSSION

5.1. INITIAL CHARACTERIZATION

Five Component alloy system is sputtered by varying the power density of different targets used during sputtering. Principle advantage of Combinatorics is exploited to achieve a systematic gradient in elemental concentration in a single sample. The quinary system is sputtered at different temperatures to investigate the formation of different phases with change in temperature.

The Figure 5-a below represents the composition profile of a gradient sample measured by Energy Dispersive Spectroscopy (EDS). Such a measurement is performed in 2 direction to analyse a gradient of Fe/Mn–Nb and Ni–Co i.e. variation of these elements in the 5 component system is analysed.

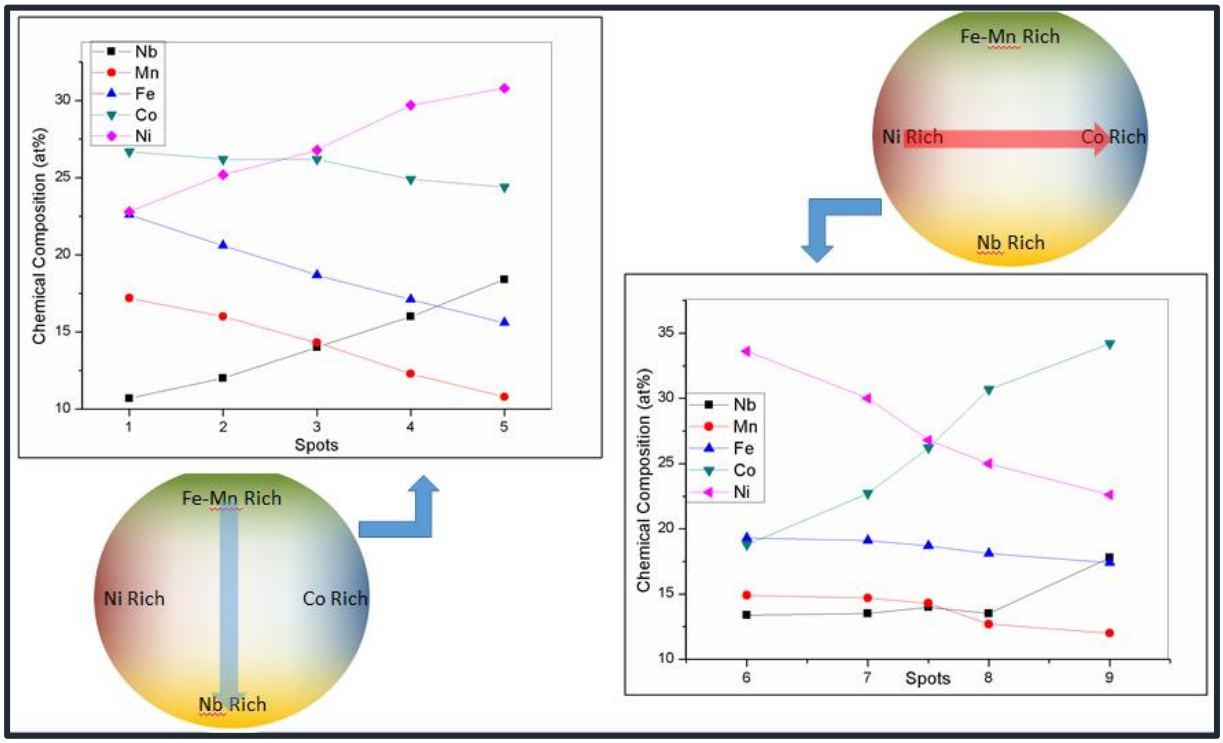

Figure 5-a EDX result of the 5 component samples, sputtered at different temperatures.

The compositions are checked for the corresponding phase formation as a function of varying temperatures during sputtering. When sputtering is carried out at room temperature, x-ray

diffractograms (XRD) show an amorphous behaviour for all the analysed composition where Nb content varies from ~11 at% to ~18 at%. Annealing treatments performed on the room temperature sputtered samples showed no indication of crystallization even after annealing at temperatures as high as 500 ˚C for 4 hours. The XRD patterns shown below are obtained for the minimum (~11 at.%) Nb concentration achieved during sputtering.

When the temperature of sputtering is raised to a values of 200 ˚C and 300 ˚C, as shown in Figure 5-b, formation of crystalline phases are observed. Because of the presence of 5 components within a single system, there are numerous possibilities for the formation of different phases or even intermetallic compounds.

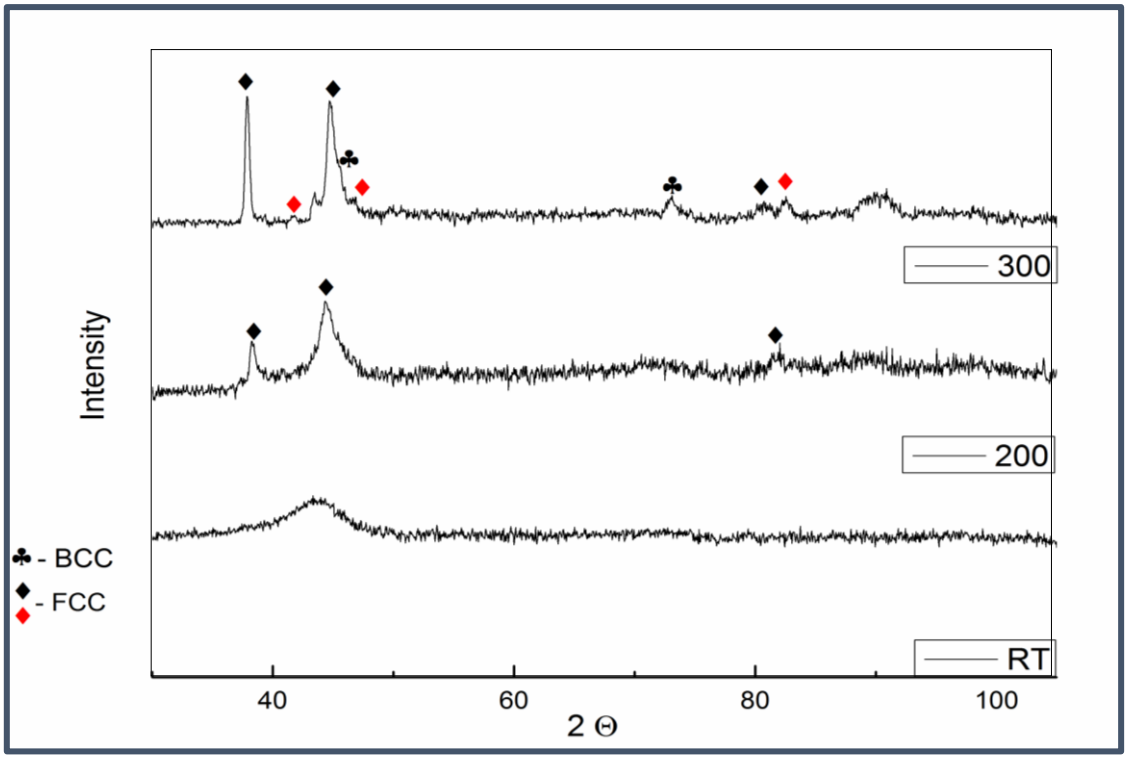

Figure 5-b X-ray diffractograms of the 5 component alloy system, showing the effect of variation in temperature.

In this case, peaks were indexed using Bragg's law, taking into account the characteristic planes of the different cubic crystal lattices. The above calculations are done considering the presence on a FCC or a BCC phase as indicated in the Figure 5-b of lattice. The elemental distribution at near atomic scale is measured using atom probe tomography.

The Figure 5-c below shows the overall elemental distribution in the 5 component system. Also, the distribution of individual elements is shown which indicates the presence of precipitates. Also there is enrichment of carbon, oxygen and silicon at the lower regions of the representative tip.

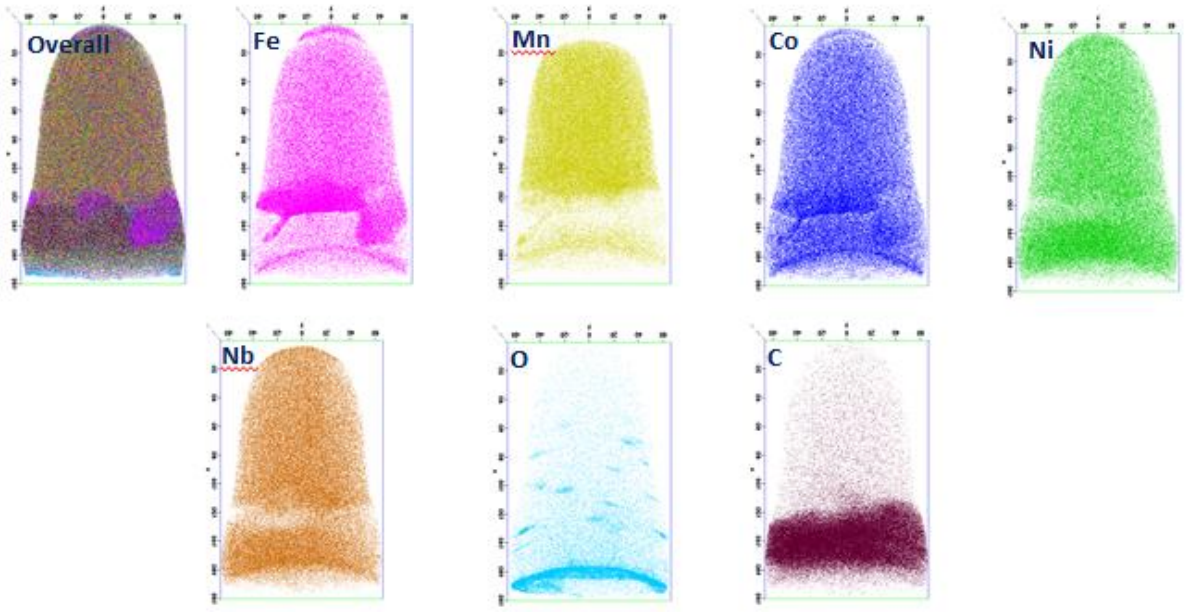

Figure 5-c Elemental distribution of the sample having composition mentioned below, from Atom Probe Tomography

The elemental concentration of the sample analyzed is shown in the table below.

Elements	Fe	Mn	Co	Ni	Nb	Si	C	O	Cr
Concentration (at.%)	16.28	7.96	24.52	27.98	11.32	11.30	0.56	0.05	0.02

1-D concentration profile is measured along the cylinder of x nm diameter, as in the Figure 5-d. It can be seen, in the matrix region. The presence of Co and Fe rich phase depleted of other elements can be visualized. It is possible that the Co-Fe intermetallic phase might have formed on increasing the temperature during sputtering.

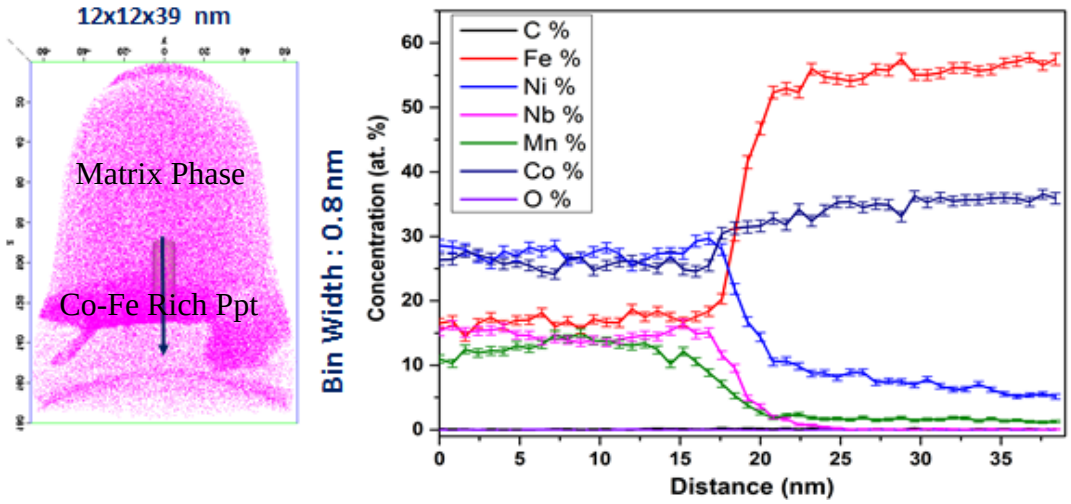

Figure 5-d 1-D concentration profile of the analyzed composition, from Atom Probe Tomography.

Further analysis was done by using transmission electron microscopy. Thin lamella was prepared using focused ion beam of Gallium ions. This so prepared lamella is analysed as shown. The Figure 5-e shows the presence of columnar grains in bright field mode, and the corresponding selected area diffraction pattern. The SADS pattern shows the presence of at least two phases with presence of additional diffraction spots from the Si substrate and does not show any particular pattern for a single phase. The grain morphology of the 2 layers is different. On performing EDS composition map of the represented area, it was found that this second equi-axed grain layer near the substrate is a result of silicide formation from the substrate due to the sputtering at high temperatures. This Silicon enrichment was also seen in the atom probe results as discussed before.

Figure 5-e Transmission Electron Microscopy of the 5 component system, sputtered at 300C.

Hence one can observe peaks corresponding to silicides and intermetallics (seen in APT) in x-ray diffractograms. Since in case of HEA, every element has its specific role to play and therefore each element affects the phase(s) formed in a system.

To study the effect of each alloying element on the phase formation, various combinations were sputtered including binary, ternary and quaternary systems before sputtering the 5 component HEA, which were of interest.

5.2. ALLOY SYSTEMS SPUTTERED

All the possible elemental combinations are mentioned in the table. The highlighted ones show the combinations that were sputtered. Some systems were crystalline at room temperature while some were amorphous, therefore heated at a higher temperature (~300 °C). These systems are discoursed in detail in this chapter. Also final High Entropy Alloy sputtered, along with its magnetic properties are discussed later in this section. However it should be noted that the targets and their positions are changed for sputtering different systems, in the sputtering chamber. The binary and ternary systems required a gradient between Fe and Mn to be studied hence individual targets used are Fe, Ni, Mn and Co. However the Quaternary and Quinary system are sputtered from a Fe-Mn alloy target, Ni, Nb and Co as there is a provision to sputter from just 4 Magnetrons at a time.

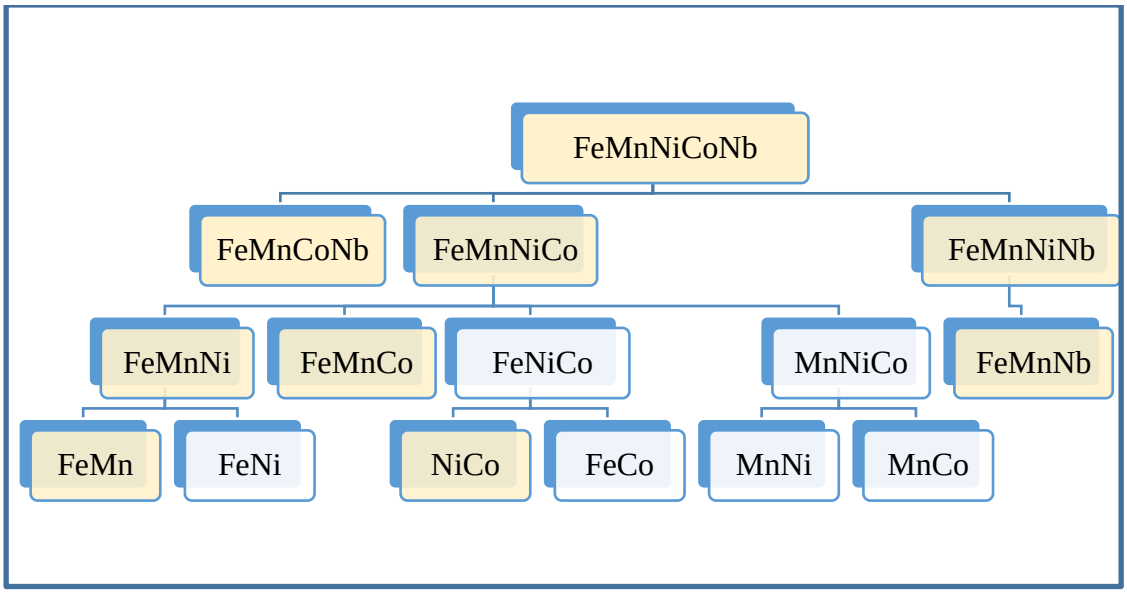

Table 5-1 Possible Binary, Ternary, Quaternary and quinary systems for the elements selected.

5.3. BINARY SYSTEMS

In the present study, Fe-Mn and Ni-Co binaries are studied in detail. Phase diagram of both the systems are shown in Figure 5-f. Information at room temperature is not available for both the systems and therefore there is an ambiguity as to what phases are present at room temperature for a particular composition.

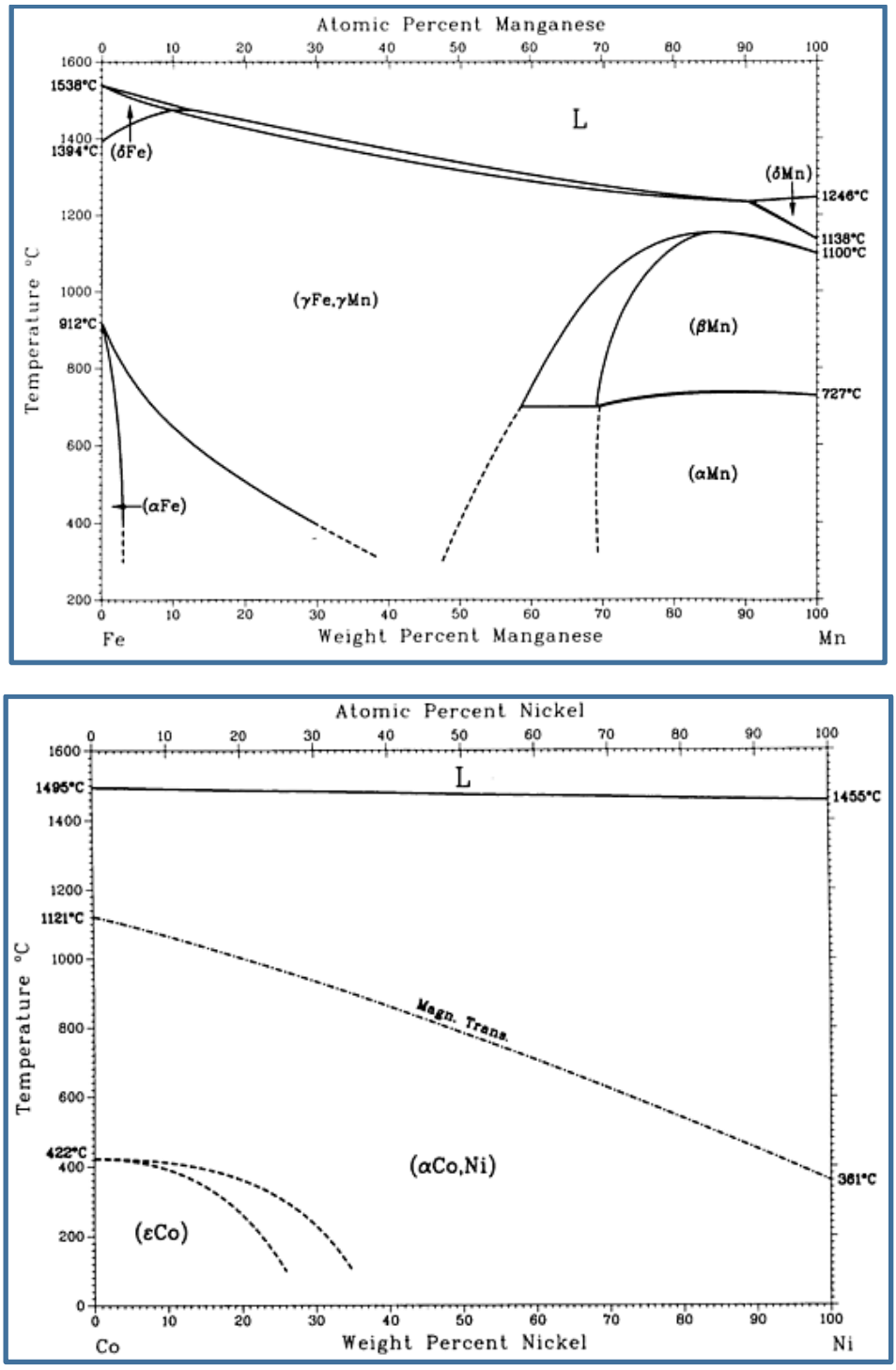

Figure 5-f Phase Diagram of Fe-Mn Binary System (i) and Ni Co Binary System (ii) showing ambiguity in phases present at Room Temperature. [33]

Various samples produced during sputtering are characterized via EDX to obtain a compositional overview. Final Composition (in at %) achieved for the binary systems Fe-Mn and Ni-Co are shown in Figure 5-g. All the samples are sputtered at room temperature.

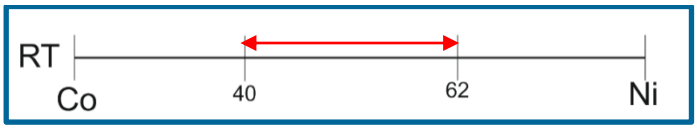

Figure 5-g Compositional overview of the Binary samples sputtered, characterized via EDX.

These compositions are analyzed by the means of X-ray diffractograms, to study the phase transformation characteristics with change in composition.

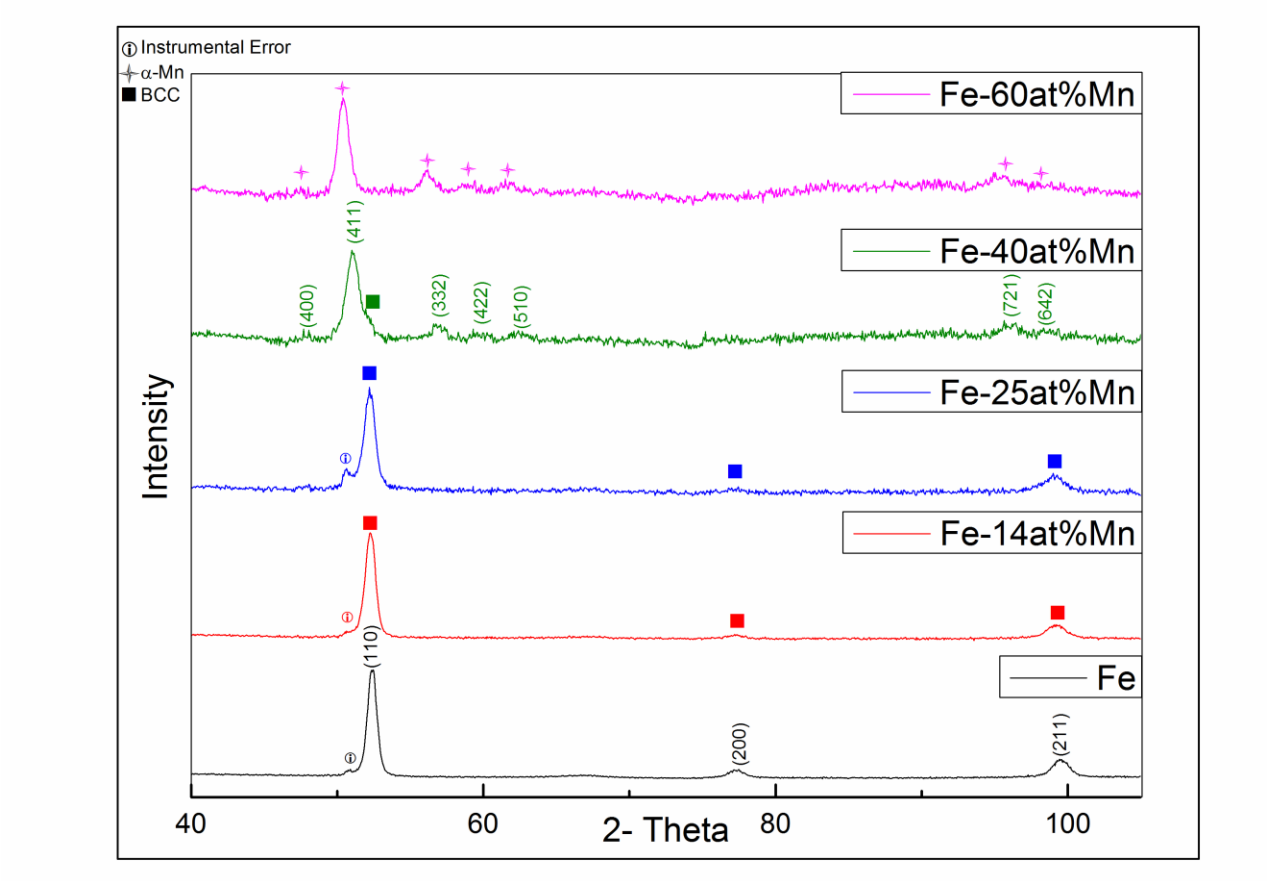

Figure 5-h XRD analysis of Binary Fe-Mn for some representative compositions.

Figure 5-h gives a brief idea of the associated phase transformation with change in Mn content for the Fe-Mn binary. X-ray diffractogram of pure Fe as shown, is a BCC lattice. Adding Mn to Fe does not lead to any phase transformation until a Mn content of ~40 at%, where a small shoulder at around 52.25° 2-theta value, divulges the presence of a BCC phase still present in small quantity.

Mn content more than 40 at% shows an α-Mn type structure. Pure Mn at room temperature has an A12 structure, α-Mn configuration. It is a complex cubic crystal structure (a= 0.892nm) consisting of 58 atoms per cell [34]. This lattice is said to have 4 asymmetric units

in a cubic crystal. This structure is evident from the diffractograms for the compositions more than 40 at% Mn.

Addition of Mn to Fe has an evident influence on the increment of the lattice parameter, seen in Figure 5-i, calculated from the x-ray diffractograms for various compositions. In a BCC lattice, on increasing the Mn content, the lattice parameter is seen to increase from that of pure Fe to a comparable value. However as soon as Mn is increased above 40 at%, this value abruptly increases from 2,89Å to a value of 8.8Å (lattice structure similar to that of α-Mn, consisting of 4 asymmetric units in the lattice). On further increasing the Mn content, the lattice parameter increases to a value similar to that of pure Mn ~8,92Å. This observation can be understood from the fact that the atomic radius of Mn is higher than Fe and any increase in Mn content would result into a lattice expansion. The abrupt change is attributed to the change in crystal structure.

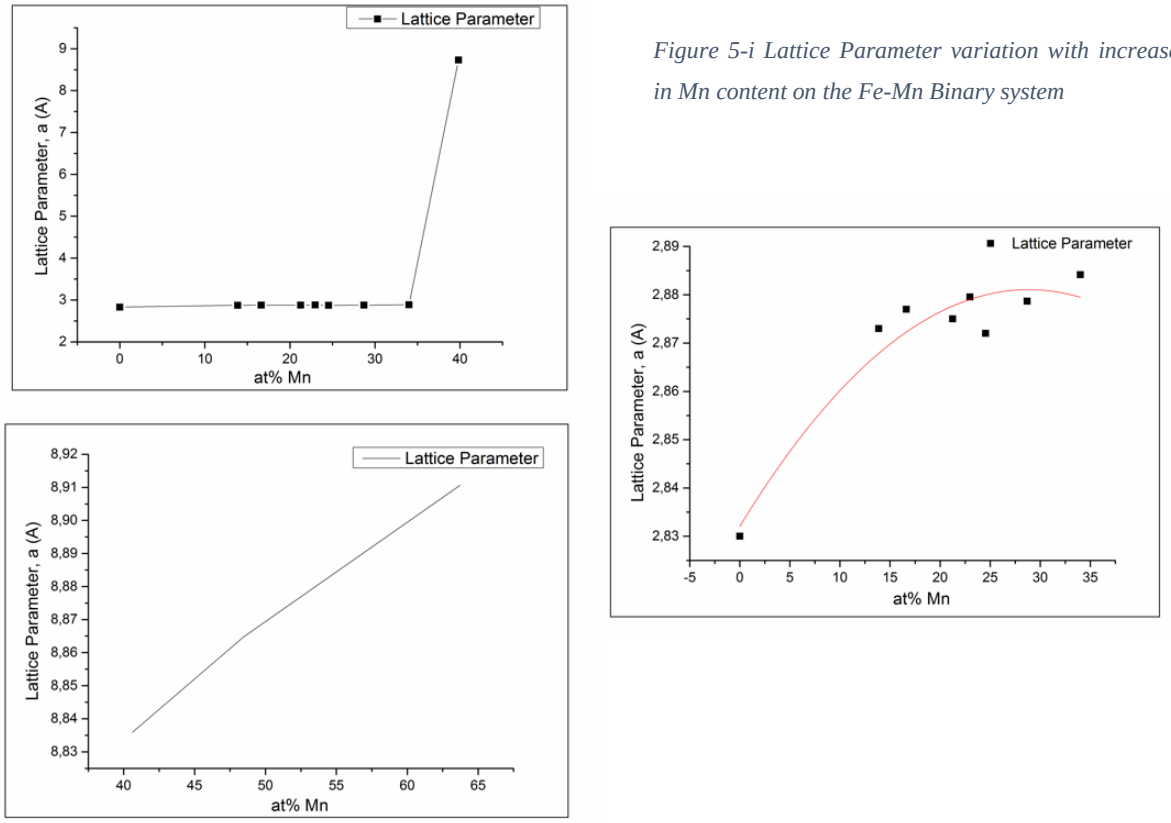

Figure 5-i Lattice Parameter variation with increase in Mn content on the Fe-Mn Binary system

Similarly Ni-Co binary system is studied using x-ray diffractogram for the various compositions achieved during sputtering. According to the phase diagram shown in Figure 5-a, there is a transformation from a FCC to a HCP phase but the exact change is not known at room temperature.

Ni-Co binary is sputtered at room temperature. The X-ray diffractogram of the representative Ni-Co compositions are shown in the Figure 5-j. It shows that a FCC phase is stable for

higher Ni content however as soon as the Co content reaches a value of 49at%, the diffractogram starts to show the appearance of a HCP phase at around 49° 2-theta value. This peak intensifies at 55 at% Co content with a visible transformation from a FCC phase to a HCP phase at around 60 at% Co.

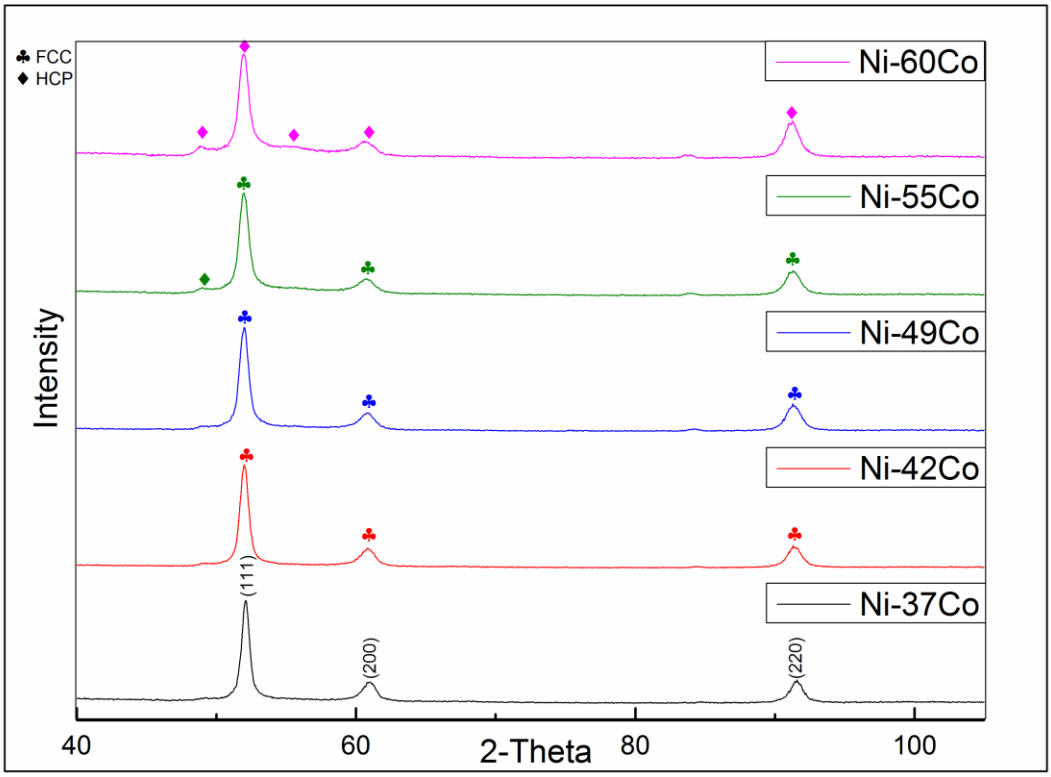

Figure 5-j XRD analysis of Binary Ni-Co for some representative compositions

The lattice parameter increases slightly with increase in Co content and further increasing the Co content leads to an appearance of an HCP phase. This dual phase structure continues to appear until 60at% Co. It is expected on further increasing Co concentration in Ni would lead to the formation of a complete HCP single phase. The slight increase in Lattice parameter with increasing Co content can be directly explained from the slight difference in atomic radius between the 2 elements.

5.4. TERNARY SYSTEM

Fe-Mn and Ni-Co binary are extended to ternary systems in order to study the effect of Ni and Co on the Fe-Mn Binary, Hence FeMnCo and FeMnNi systems are sputtered and analyzed. Co and Ni content were varied and the chemical composition was measured via EDX.

Figure 5-k shows X-ray diffractogram of some representative compositions (compositions achieved represented in Figure 5-l) for both the ternary systems. These compositions are chosen to represent the highest and lowest Ni/Co contents achieved during sputtering that is, it briefly illustrates the phase formed within the given composition range achieved.

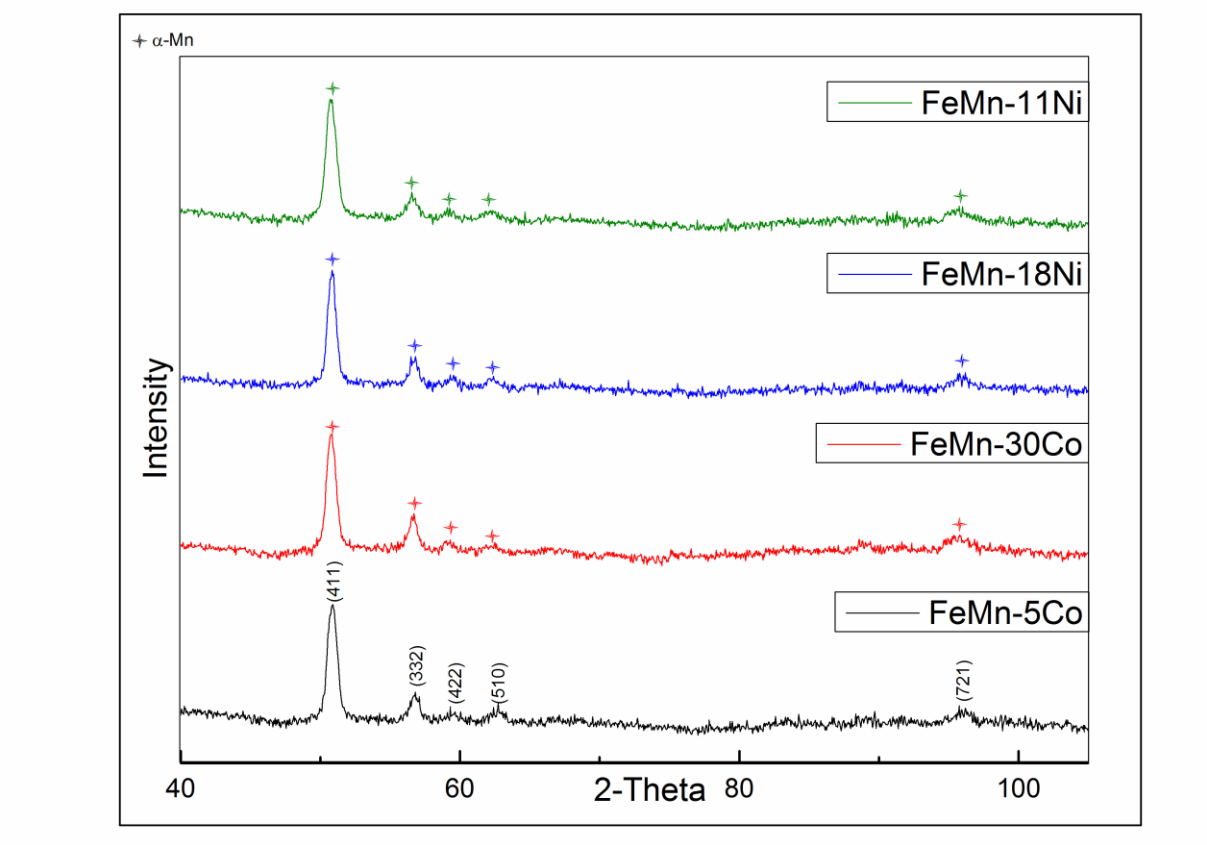

Figure 5-k XRD analysis of Ternary FeMnNi and FeMnCo for some representative compositions

The diffractogram clearly shows that on addition of Ni and Co in the Fe-Mn binary system, it still forms α-Mn structure. Figure shows the achieved compositions, during sputtering for the ternary system measured via EDX. Both FeMnNi and FeMnCo show the presence of α-Mn structure in this range and no change in crystal structure is observed throughout the sputtered composition.

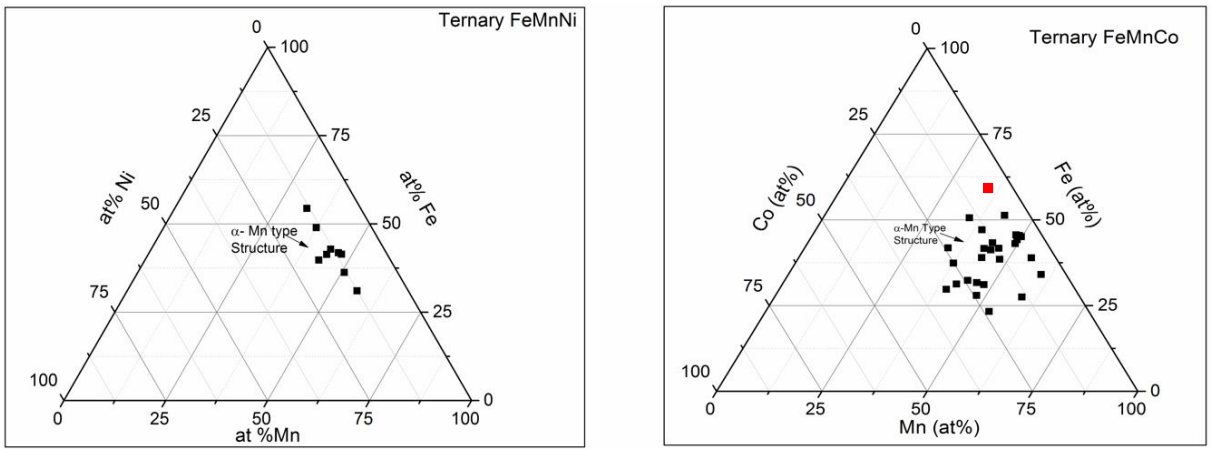

Figure 5-l A Ternary plot to depict the composition of the 2 ternary systems achieved during sputtering analyzed via EDX.

According to the known fact, Ni, Co and Mn when added to Fe stabilize the γ (FCC) phase rather than α (BCC) phase. Here, as one can see addition of these elements does not allow the BCC phase to get stabilized, neither do they stabilizes an FCC phase with these compositions as Mn has a more pronounced effect in stabilizing the α-Mn structure. In fact Ni and Co tend to stabilize the system with the α-Mn structure even at a lower Mn content.

Consider a composition (Fe-59.24 Mn-35 Co-5.76 at %) marked (with red) on the ternary plot for FeMnCo (Figure 5-l). This composition is a good example to represent the lowest Co content which stabilizes α-Mn structure with the lowest Mn content achieved. From the Binary Fe-Mn samples, it was evident that the BCC phase transforms to an α-Mn structure at around 40at% Mn, still with some BCC phase present This transformation point is lowered to around 37at% Mn-Fe (considering relative atomic concentrations of Fe and Mn in the same ternary system) by adding just around 6at% of Co.

However it is expected (from what is already known and evidence from the Ni-Co system studied) with lower Mn contents and increased Ni/Co contents, a FCC phase can be stabilized and a further increase in the Co content can initiate the appearance of a HCP phase. However there are no experiments conducted in this respect during the study and proofing this statement can be of future interest.

Lattice parameter calculation of some representative compositions are shown in Figure 5-m, to give a gist of the elemental contributions.

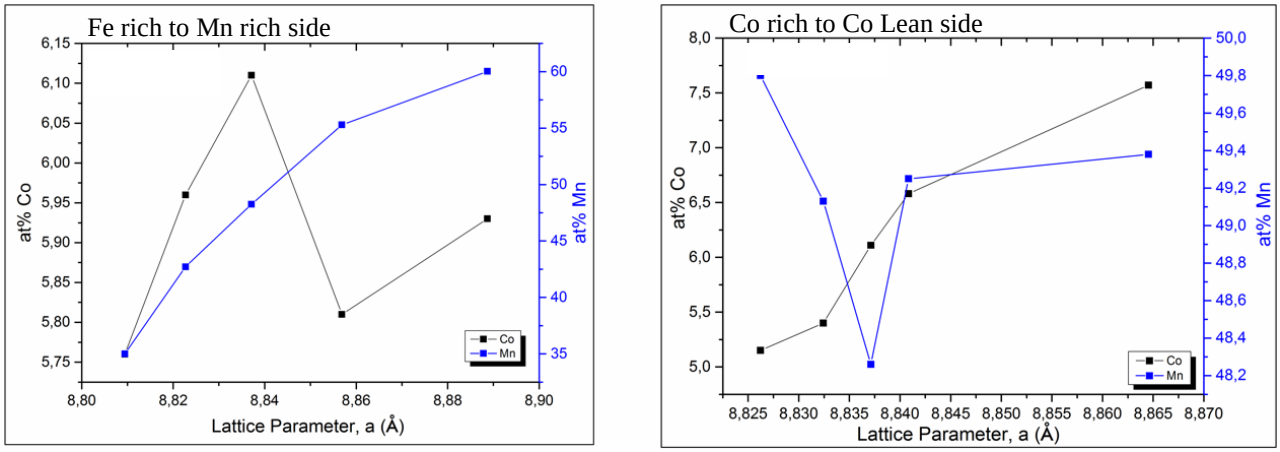

Figure 5-m Change in Lattice Parameter with change in elemental composition (as a function of Mn and Co contents)

These graphs are plotted so as to observe a variation in lattice parameter with respect to one element (Mn/Co) while the other is almost constant (Co/Mn). Figure 5-m–i shows an increment in lattice parameter with increase in Mn content while the same is observed with increase in Co content on the other graph. Increase in lattice parameter can be said to have contributions from both the elements, however Mn is observed to have a higher influence on this characteristic. This can be well understood from the atomic radii values of the 2 elements. Atomic radius of Co is more than Fe but not as much as Mn. A similar trend can be observed in FeMnNi system where both the elements lead to a net increment in the lattice parameter.

5.5. QUARTERNARY SYSTEM

FeMnCoNi system is sputtered and analyzed to study the phase that will be stabilized when all these elements are put together to form an equiatomic alloy system. Until now it was known that Fe has a tendency to stabilize the BCC phase below 40% Mn in the Binary Fe-Mn system, above which α-Mn structure is a stable phase. Ni and Co stabilize the FCC phase until Co content reaches around 50 at%, where HCP phase starts to appear and further increment leads to the stabilization of this phase. For the ternary systems, for the achieved composition, it is also very much evident that addition of both Ni and Co does not stabilize the BCC phase; instead they lower the transformation point in favor of α-Mn structure.

Keeping the above results in mind, quaternary FeMnCoNi is sputtered and the Compositional analysis of the sample via EDX is represented in the schematic as shown in the Figure 5-n (Inset shows a representation of the expected chemical gradient). However one should keep in mind that the setup of the targets for sputtering is changed. Fe-Mn (50-50at %) alloy target is used instead of using Fe and Mn targets separately. Therefore the focus is on achieving an equiatomic composition, instead of achieving the Fe/Mn gradient in the quaternary system.

However it is necessary to study Ni/Co gradient as their binary shows a second phase emergence near equiatomic composition.

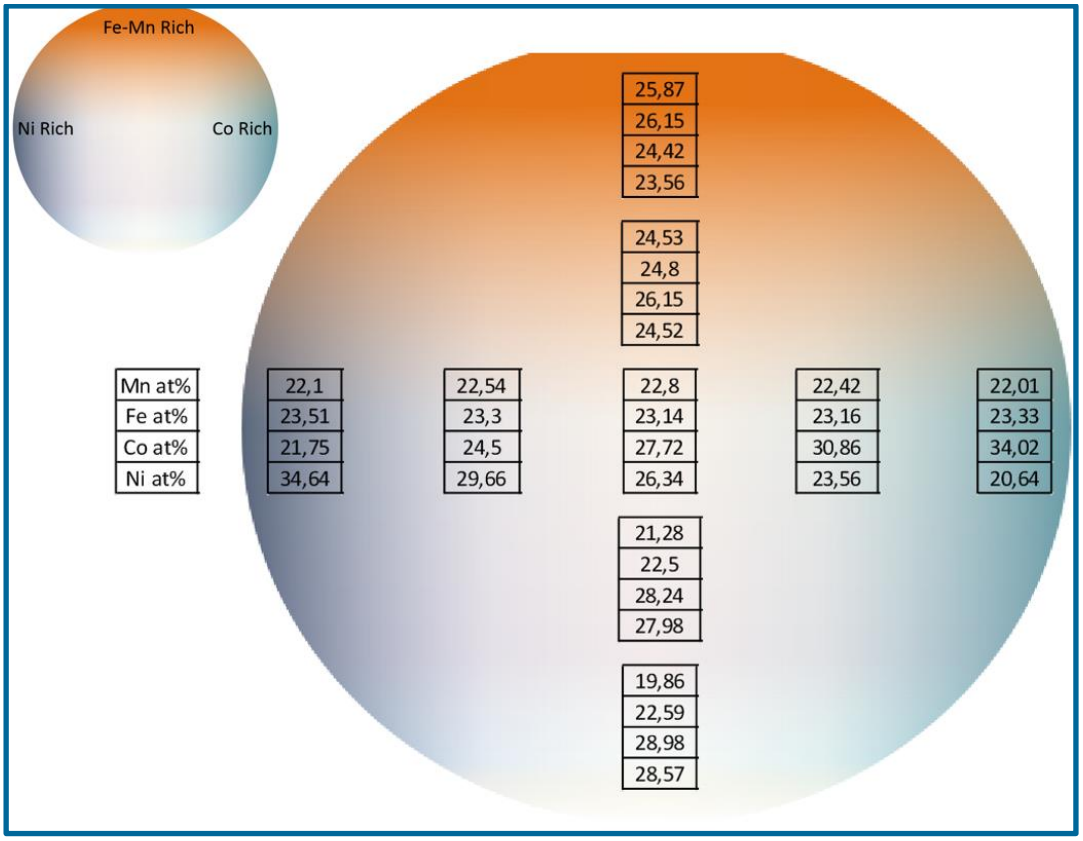

Figure 5-n EDX analysis showing composition change in a combinatorial sample of the 4 component system

On these spots, x-ray diffraction patterns are obtained which are shown in Figure 5-o. The spots are identified according to what has been discussed previously in section 4.2, Figure 4-d.

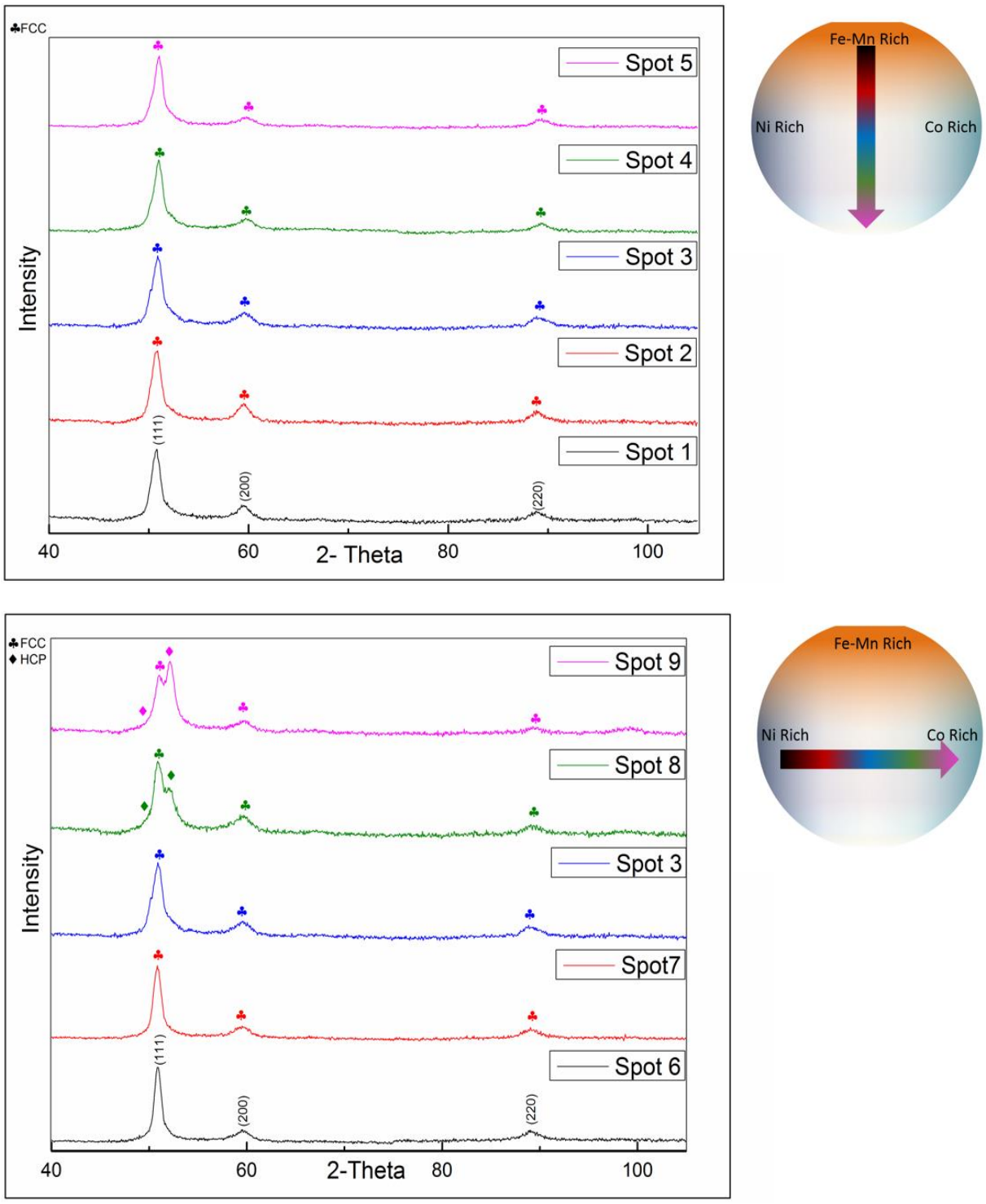

Figure 5-o XRD analysis of Quaternary FeMnNiCo system for the composition represented in the previous EDX plot.

On moving from spot 1 to spot 5 i.e. from Fe/Mn rich region to Fe/Mn lean region, one can see a single FCC phase has been depicted by the diffractograms. Similarly on moving from spot 6 to spot 9 i.e. from a Ni rich region to Co rich region, one can perceive a single FCC phase until Co content reaches a value of approximately 30 at%, where appearance of a second phase HCP structure is noticed. On increasing the Co content, this HCP phase fraction increases, as observed from the increase in intensity of the HCP diffraction peak, ref spot 9.

This observation fits very well to the experiments, on the binary and ternary systems. Phase separation on increasing the Co content has been seen before, which is once more discernible in the quaternary system. There is no noticeable change in the lattice parameter and the average estimated value from x-ray diffraction, is equal to 3.6 Å.

5.5.1. ELEMENTAL DISTRIBUTION AT NANO SCALE VIA ATOM PROBE TOMOGRAPHY

The composition for spot 8 i.e. Mn-22.42 at%, Fe-23.46 at%, Co-30.86 at% and Ni-23.56 at% is further analyzed to verify the composition and prove the phase separation occurring as seen in the x-ray diffractograms (showing a HCP phase). Figure 5-p shows the elemental distribution of the constituting elements. One can easily find some regions rich in Co while other regions rich in the remaining elements.

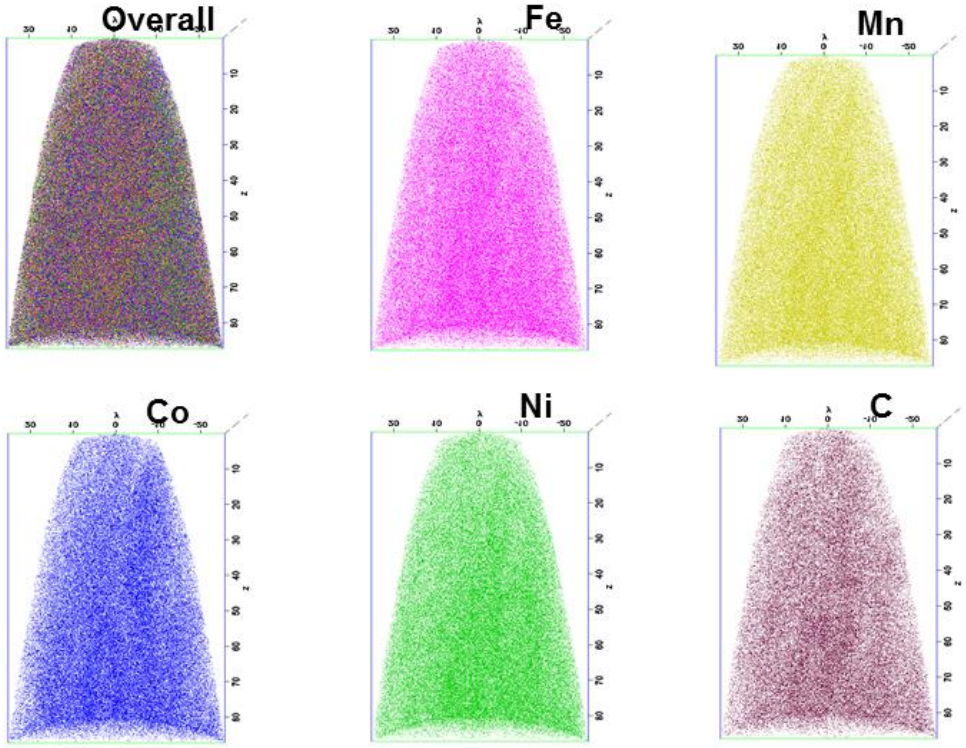

Figure 5-p Elemental Distribution of all the components of the quaternary system

Further analysis via 1-D concentration profile of the selected cylindrical region of interest as shown in Figure 5-q. On moving in the direction of the arrow shown, there is an increase in Co content from around 23 at% to around 45 at% while the other elements seem to be enriched and depleted concurrently. One can easily infer from such information that increasing the Co content results into HCP phase separation rich in Co.

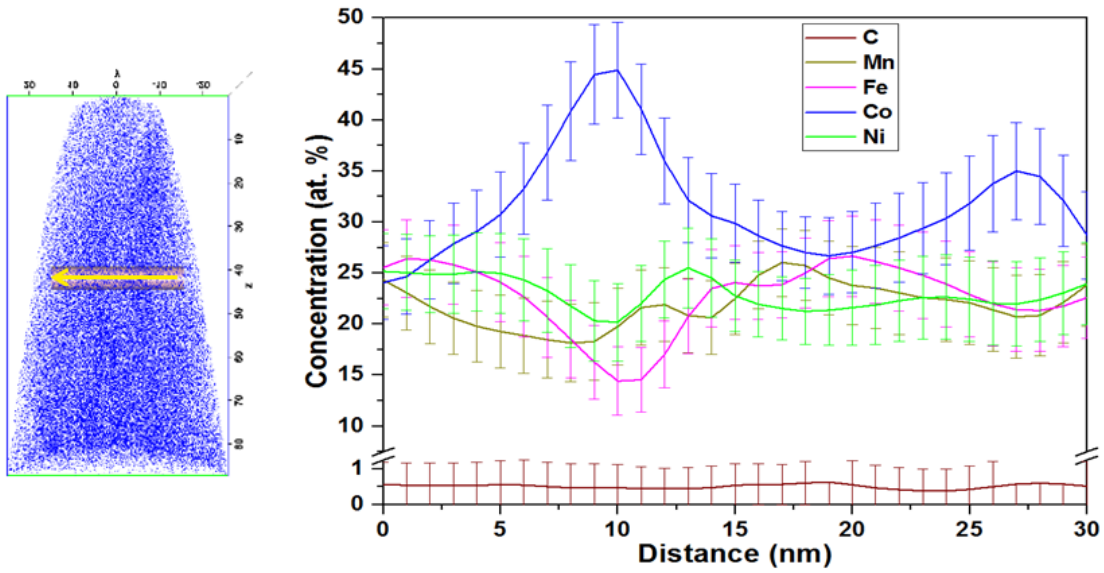

Figure 5-q 1-D Concentration Profile of all the components on the quaternary system, Atom Probe Tomography.

Another quaternary FeMnNiCo composition is sputtered in order to check the consistency of results as observed in the previous section. Hence the composition is slightly varied by changing the power applied to each target. The Co content is increased; simultaneous to this increase, Fe-Mn content is decreased. The EDX composition of the sample is represented in Figure 5-r. Co is varied from approximately 23 at% to 40 at% while Mn from 13 to 19 at%.

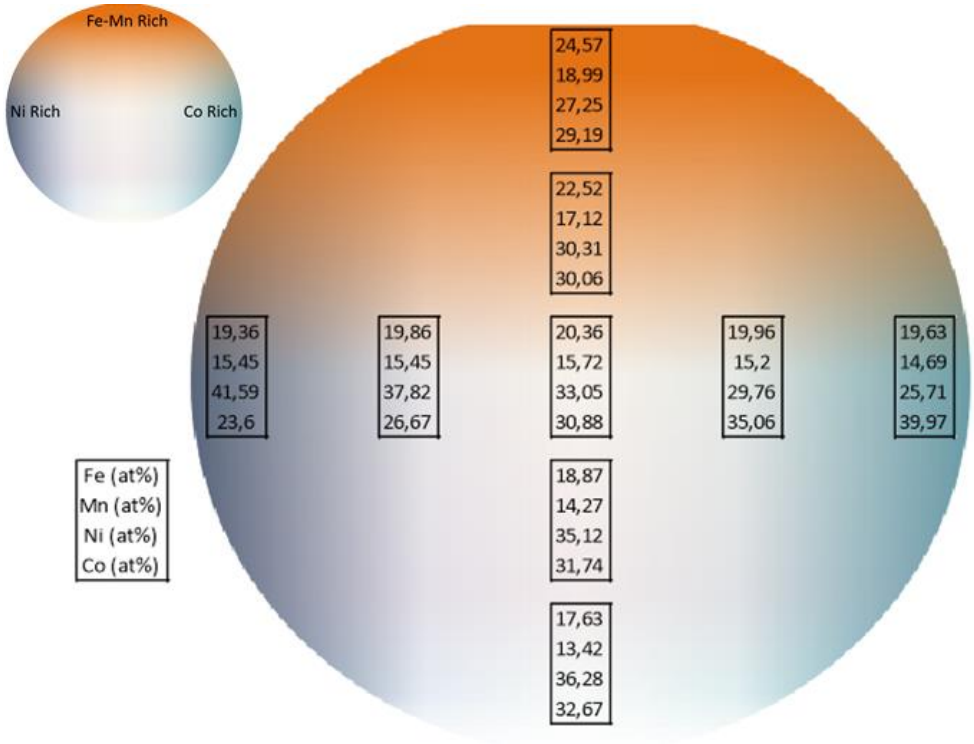

Figure 5-r EDX analysis showing composition change in a combinatorial sample of the 4 component system

X-ray diffraction patterns are taken on these spots to analyze the phase formed as shown in the Figure 5-s, shown below.

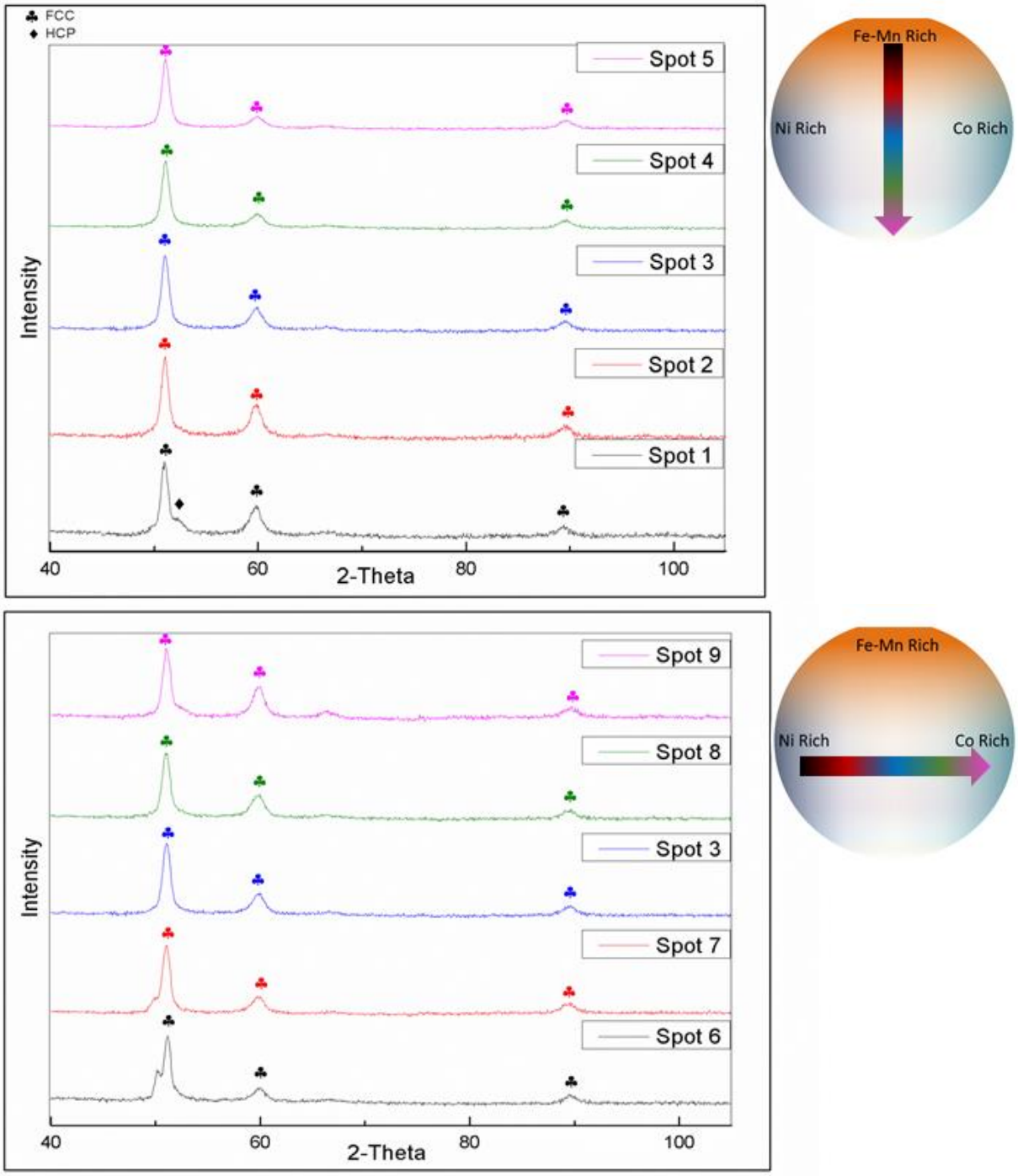

Figure 5-s XRD analysis of Quaternary FeMnNiCo system for the composition represented in the previous EDX plot.

On moving from spot 1 to spot 5 i.e. Co content of 29 at% to 32at% there is a single FCC structure except for spot 1 where a shoulder to the 1st peak depicts the presence of another phase- HCP structure. This observation is not in correlation with the results achieved previously. On moving from spot 6 to spot 9, there is an increase in Co content from 23 at%

to 40 at%. Still the diffractograms show a consistent FCC phase to be present throughout the sample. In comparison to the previous sample, there is also a decrease in Mn content. At spot1, the Mn content is around 19 at% where Co shows phase separation. All the other compositions have Mn content quite lower to this value. One can infer that Mn aids Co to phase separate and form a HCP second phase above a certain concentration i.e. Co tends to form a HCP second phase above 30 at% only when Mn content is above 18 to 19 at%. When this condition is not satisfied the Quaternary FeMnNiCo phase tends to form a single FCC phase, evident from the above x-ray diffractograms.

5.6. ALLOY SYSTEMS WITH NIOBIUM AS ONE OF THE CONSTITUENT

Until now we have discussed phase formation in different alloy systems without considering Nb addition to any of the systems and the role of each constituent except Nb, is well discussed and understood.

The target positions and use of Fe-Mn alloy target used during sputtering, is discussed previously and the same is applied in all the systems having Nb as one of the constituents.

We shall proceed first with the FeMnNb ternary system. Figure 5-t shows the achieved composition during sputtering, measured via EDX. The chemical composition of Fe and Mn is almost equiatomic while the Nb content is varied by changing the applied voltage during sputtering. As represented in the diagram Nb content ranges from 7 at% to 43 at%.

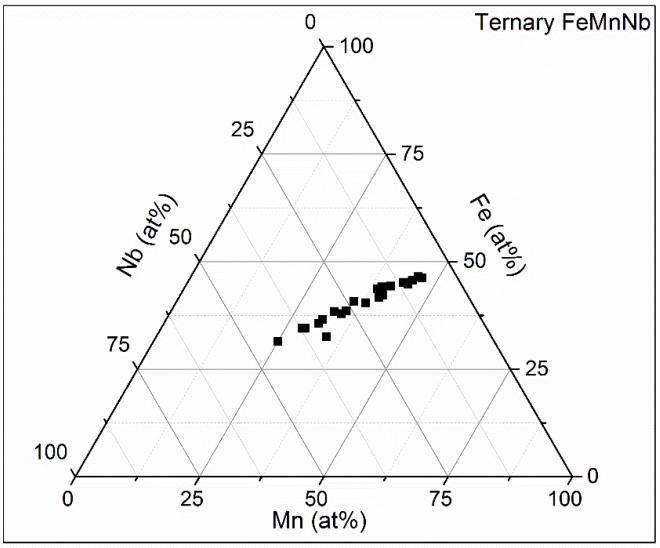

Figure 5-t Ternary plot to depict the composition of the FeMnNb ternary systems achieved during sputtering analyzed via EDX

These compositions are investigated via X-ray diffractometer to analyze the phase formed in the alloy system. It was found that on adding Nb to Fe-Mn binary, the system transforms from a crystalline α-Mn structure to an amorphous structure. Since all these analyzed samples were

sputtered at room temperature, efforts were made to obtain a crystalline state by increasing the substrate temperature to first 200 and then to 300 °C, during sputtering. Even with a Nb content as low as 7 at% and an in situ sputtering temperature of 300 °C the amorphous structure remained stable. Reason behind choosing just this temperature and not increasing the temperature any further, is explained later in this chapter during the discussion for the Quinary system.

Ternary systems of FeMnNi and FeMnCo are extended to form quaternary alloy systems by adding Nb. FeMnNiNb and FeMnCoNb are measured for their chemical compositions via EDX and the phase formed is checked via X-ray Diffraction, shown in Figure 5-u. Still the structure appears to be amorphous and increasing the substrate temperature to 300 °C does not affect any change. All these studies persuasively prove that Nb has a strong tendency towards amorphization, when studied as a constituent in a ternary or quaternary system. With an Equiatomic five component alloy FeMnNiCoNb system, the results weren't any different as shown in the x-ray diffractograms below.

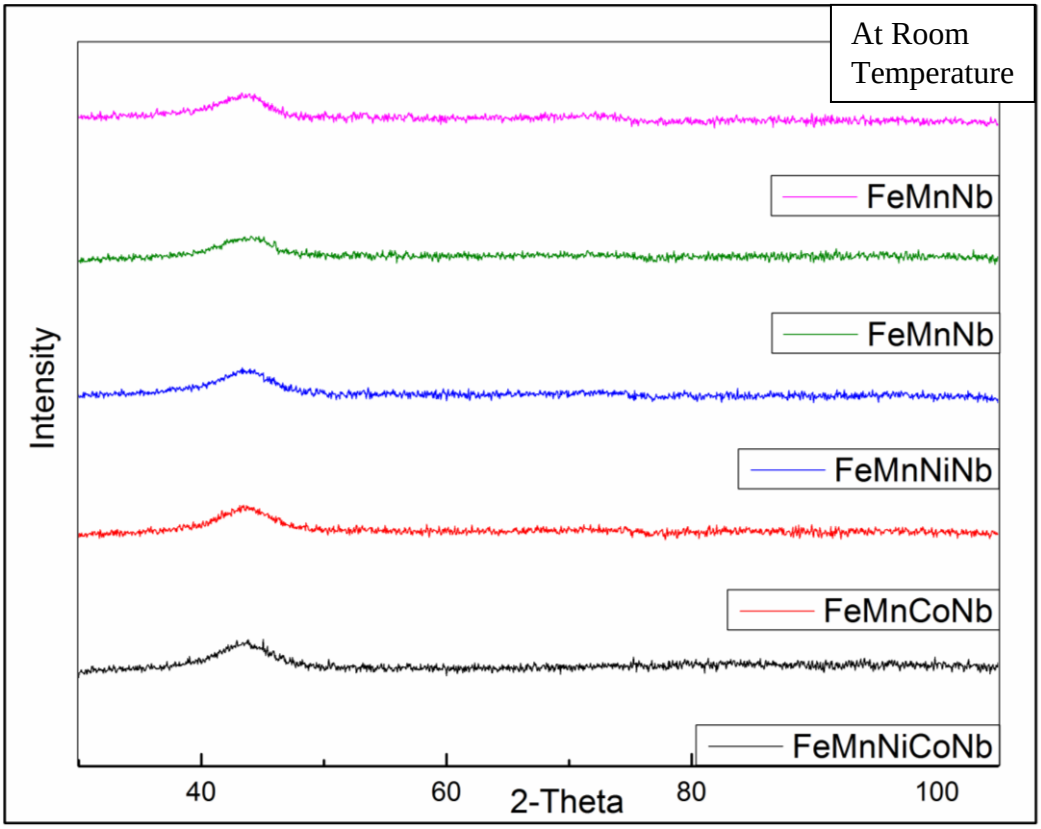

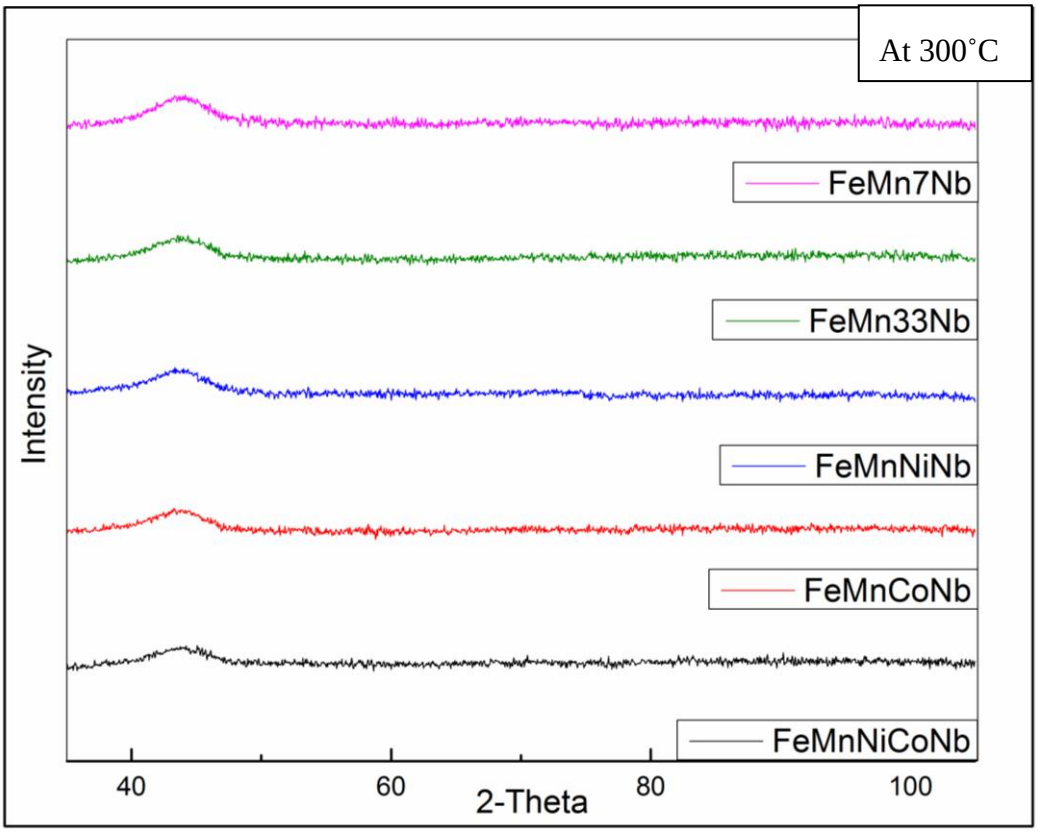

Figure 5-u XRD analysis of the alloy systems having Nb as one of the component for some representative compositions

This behavior can be partially explained by Inoue's empirical rules for glass formation which are stated as follows: [35]

- A multicomponent alloy system- An amorphous phase is likely to form on increasing the no. of components, at least 3 components.
- Higher atomic radii difference
- High negative heat of mixing, between the components favors an amorphous structure.

These rules can be verified from the fundamental properties of the constituting elements referred in Table 3-2 Fundamental properties of the elements.. Thus all these factors result in decreased diffusivity of the constituting atoms which hinder them to order themselves into a crystalline lattice thus favoring an amorphous structure.

5.7. QUINARY SYSTEM

In the previous section we discussed the addition of Nb to Fe-Mn binary, FeMnNi Ternary and FeMnCo Ternary system and concluded that Nb has a high tendency towards amorphization of these crystalline alloy systems. We now proceed towards the 5 component

system i.e. addition of Nb to the quaternary FeMnCoNi system which was seen to be a single FCC phase when having concentrations of each element, close to equiatomic values.

When this 5-component system is sputtered at room temperature, it again leads to the formation of an amorphous structure (evident from the x-ray diffraction studies) which has been observed until now for other systems. Fe, Mn, Co and Ni were almost equiatomic and Nb was varied from 12 to 18 at% (compositional analysis via EDX). In search of a crystalline phase with Nb as a constituent, efforts were made to increase the substrate temperature to 300 °C. Also this time the Nb concentration was kept to a minimum by decreasing the power applied to the Nb target. This sputtered sample was analyzed via EDX and the compositions on different spots are represented in the Figure 5-v.

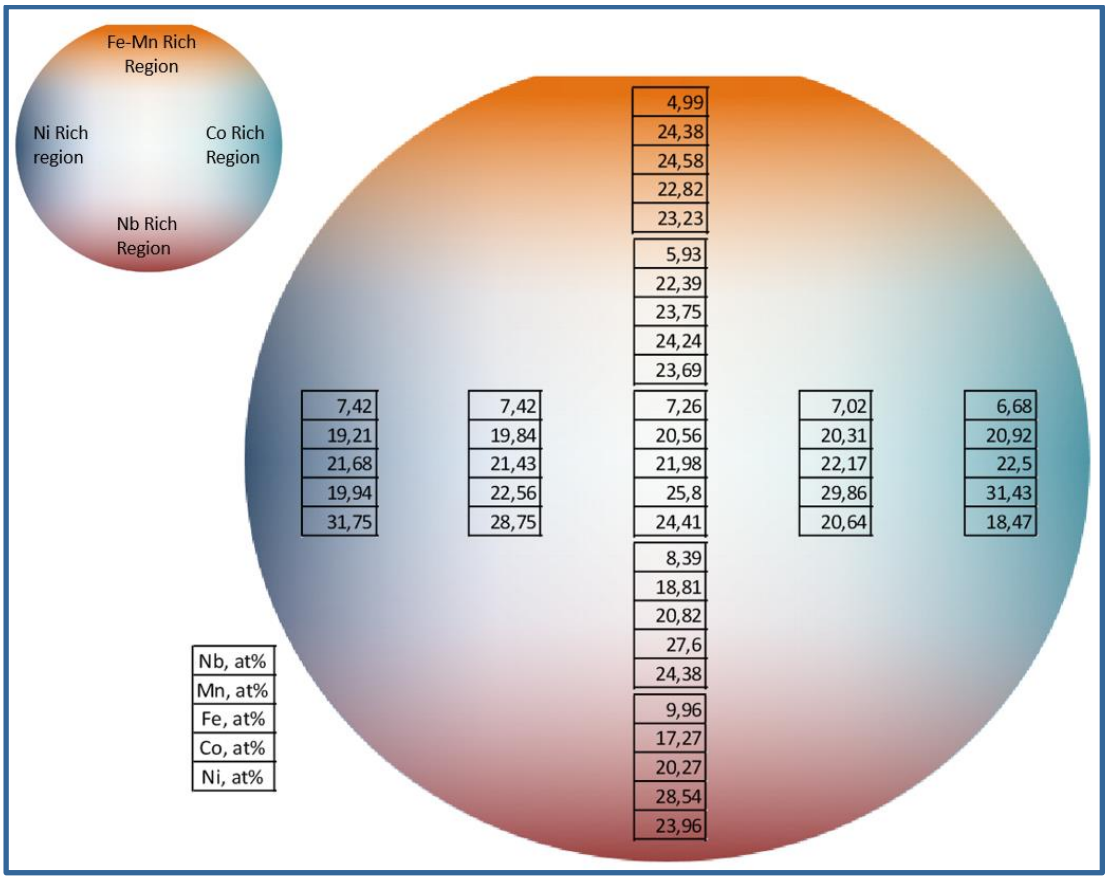

Figure 5-v EDX analysis showing composition change in a combinatorial sample of the 5 component system, sputtered.

As one can see, Nb content is varying from approximately 5% to 10%, every other element shows a variation from 20 to 30 at% approximately. Close to equiatomic compositions for the other 4 elements were also achieved; refer spot 1 and spot 2 in the schematic. These spots were investigated for the presence of any crystallinity, via X-ray Diffraction. Figure 5-w shows the x-ray diffractograms of all these spots.

From these diffractograms in Figure 5-w, one can easily spot a crystalline structure that has been stabilized by the addition of Nb to the FeMnCoNi quaternary system. However this system again shows an amorphous behavior at a Nb content of approximately 10 at% and all the compositions that were sputtered targeting a Nb content higher than this, also showed an amorphous structure. Nb content at and below approximately 9 at% shows a BCC single phase with a lattice parameter of 2.95 Å, as estimated from the diffractogram. The diffractogram also shows the samples to be textured along (211).

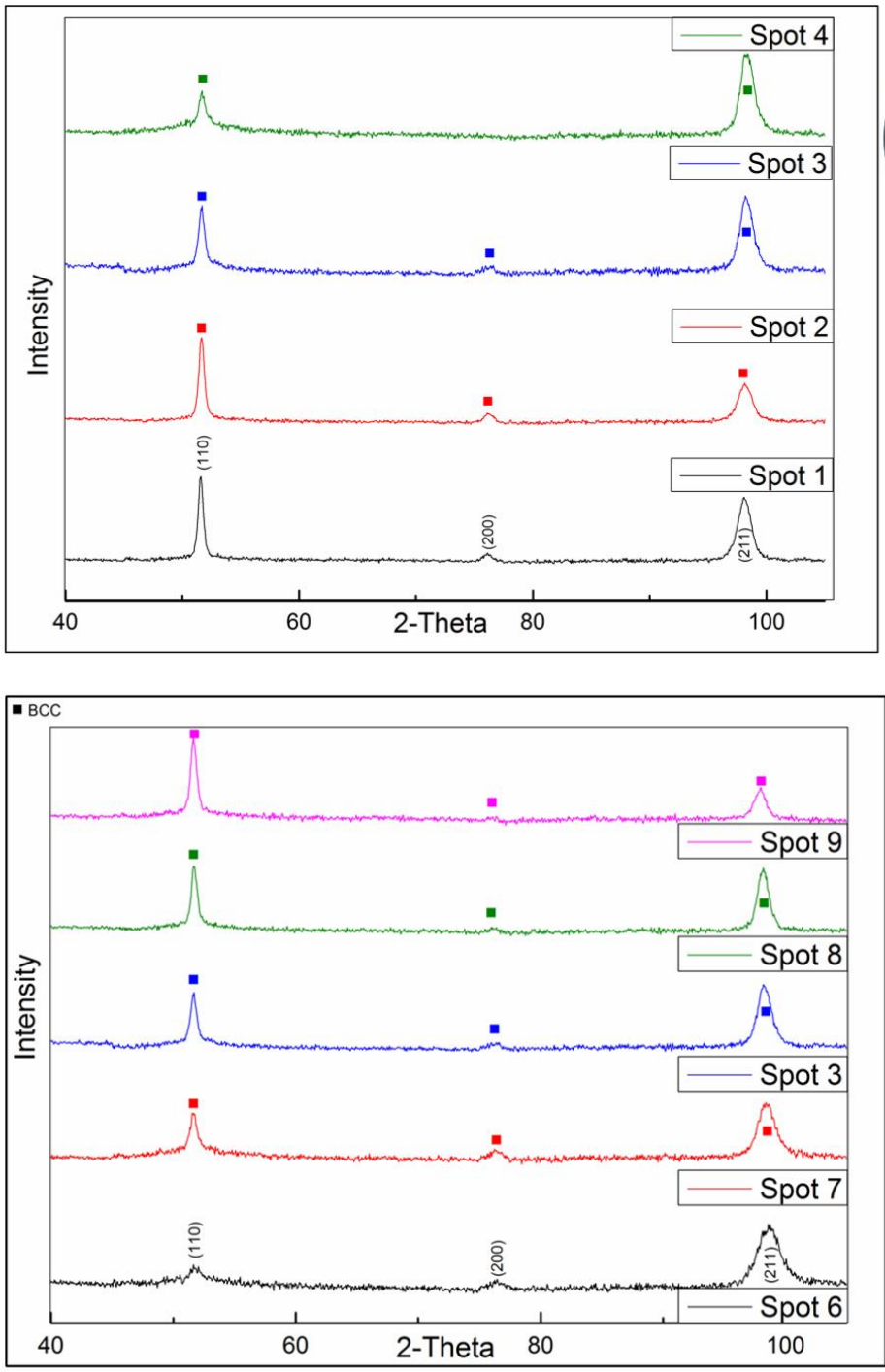

Figure 5-w XRD analysis of Quaternary FeMnNiCo system for the composition represented in the previous EDX plot.

Figure 5-x shows the hardness and reduced modulus values obtained from these spots. Hardness values also predict the presence of a different phase, on moving from spot 1 to spot 5. Spot 5 shows a sudden change in hardness and reduced modulus values with a higher deviation in the hardness and reduced modulus values as seen from the error bars, depicting the standard deviation.

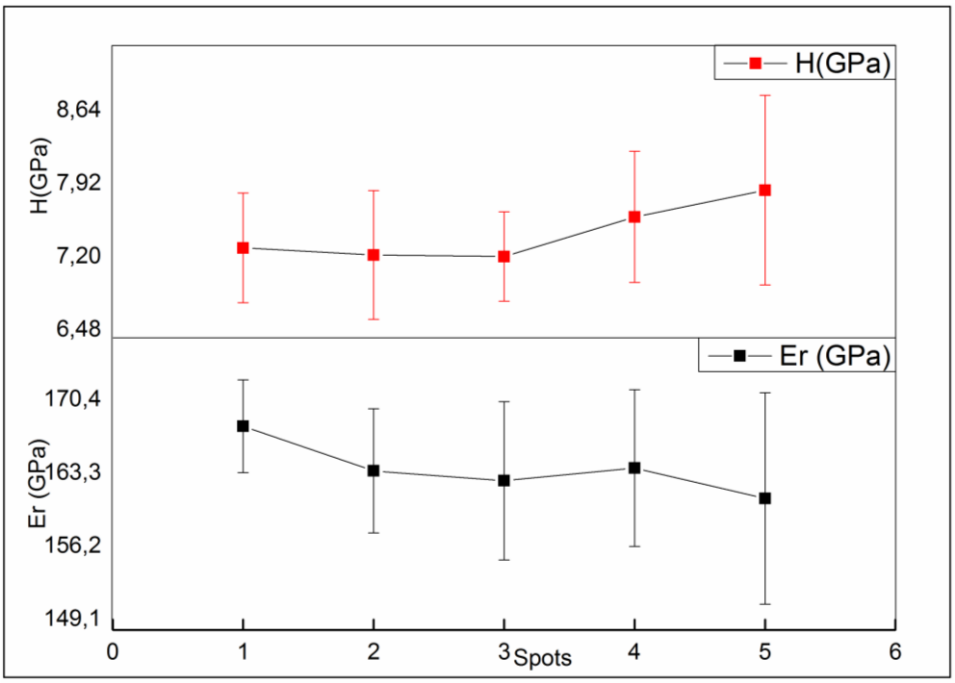

Figure 5-x Hardness and Elastic modulus measured on the 5 component FeMnNiCoNb Sample

5.7.1. ELEMENTAL DISTRIBUTION AT NANO SCALE VIA ATOM PROBE TOMOGRAPHY

The elemental distribution is checked for a homogeneous distribution at a nano scale for a representative composition via Atom Probe Tomography. Table represents the composition that had been analyzed via APT, a Nb content of 5.29 at%.

Elements	Fe	Mn	Co	Ni	Nb	C	O	B	H
Concentration (at %)	23.44	24.45	24.00	21.17	5,29	1,42	0.07	0.011	0.13

Figure 5-y shows the overall distribution of all the elements, which looks almost homogeneous. On taking a closer look at the distribution of each element, one can see some regions rich in C due to the contamination from the sputtering chamber; however these regions are too minute to be detected in the x-ray diffractograms.

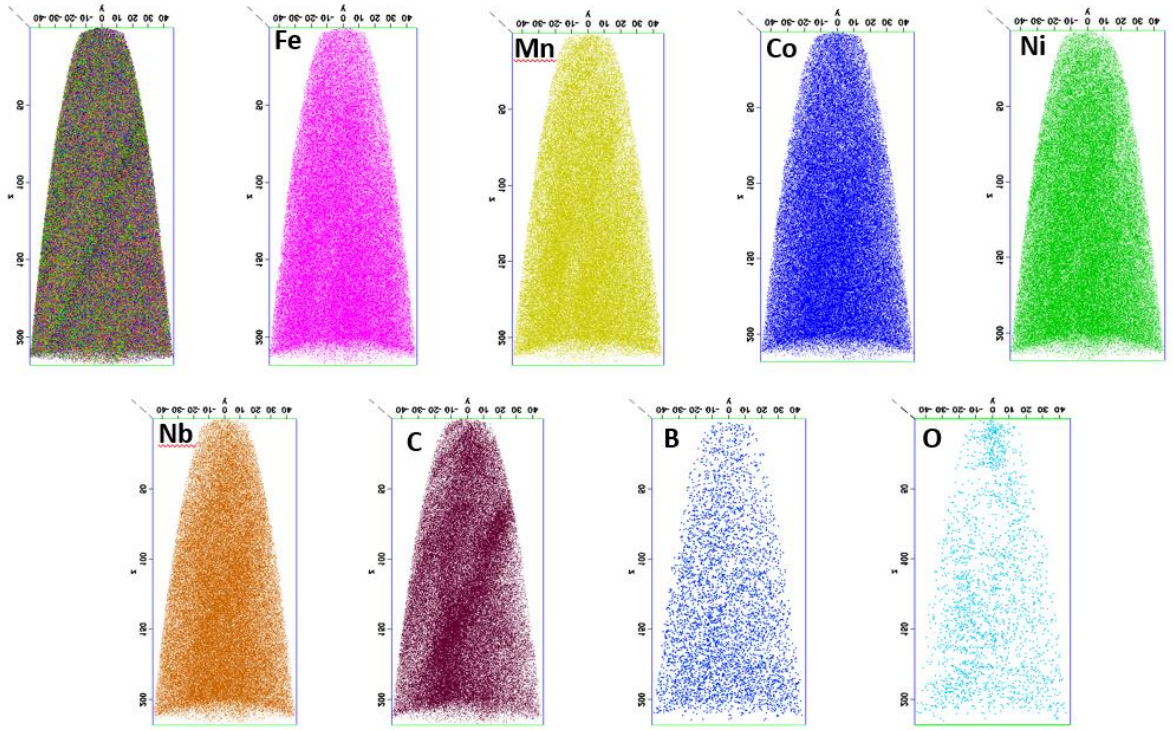

Figure 5-y Elemental Distribution of all the components of the quaternary system, Atom Probe Tomography.

Figure 5-z shows the 1-dimensional concentration profile of the elements as analyzed by APT. A cylinder of the dimension 10X10X50nm is chosen as represented in Figure 5-z, represents the concentration profile for the representative cylinder. As one can see, all the elements are distributed randomly without showing preference towards a particular element or site.

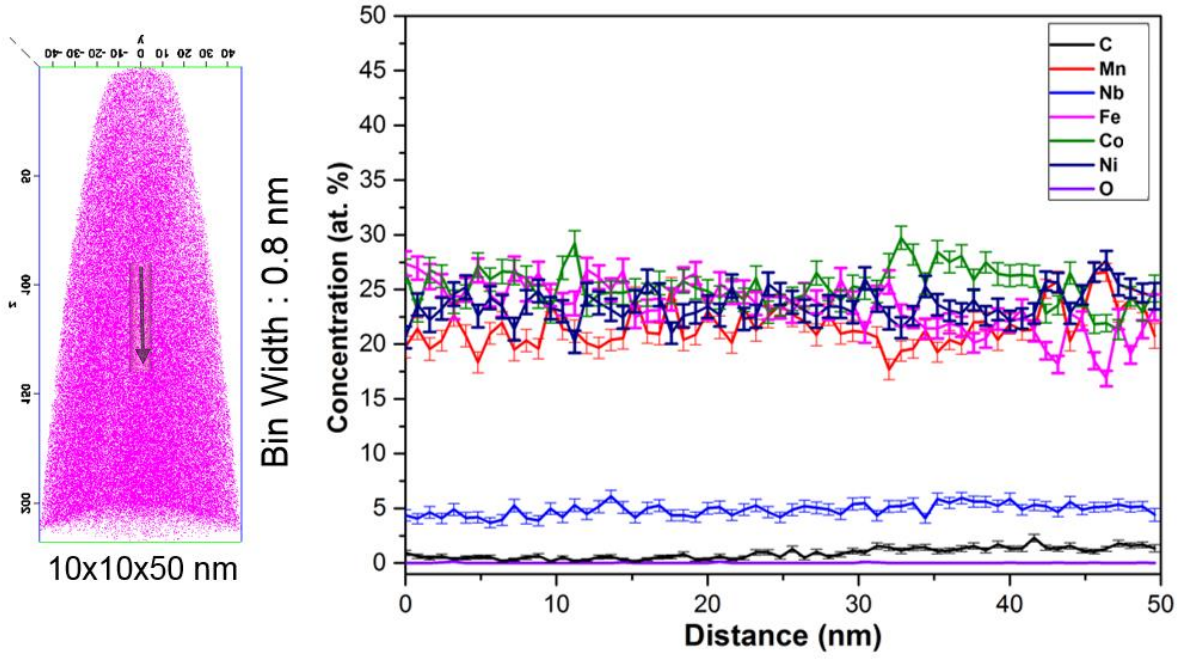

Figure 5-z 1-D Concentration Profile of all the components on the quaternary system, Atom Probe Tomography.

These results effectively show the homogeneous distribution of all the elements with some exceptions to C enriching the grain boundaries, present due to the contamination. This composition is further analyzed by Transmission Electron Microscopy. TEM lamellae are made using focused ion beam. Figure 5-aa shows the image of the lamellae in a bright field mode, with the corresponding selected area diffraction pattern.

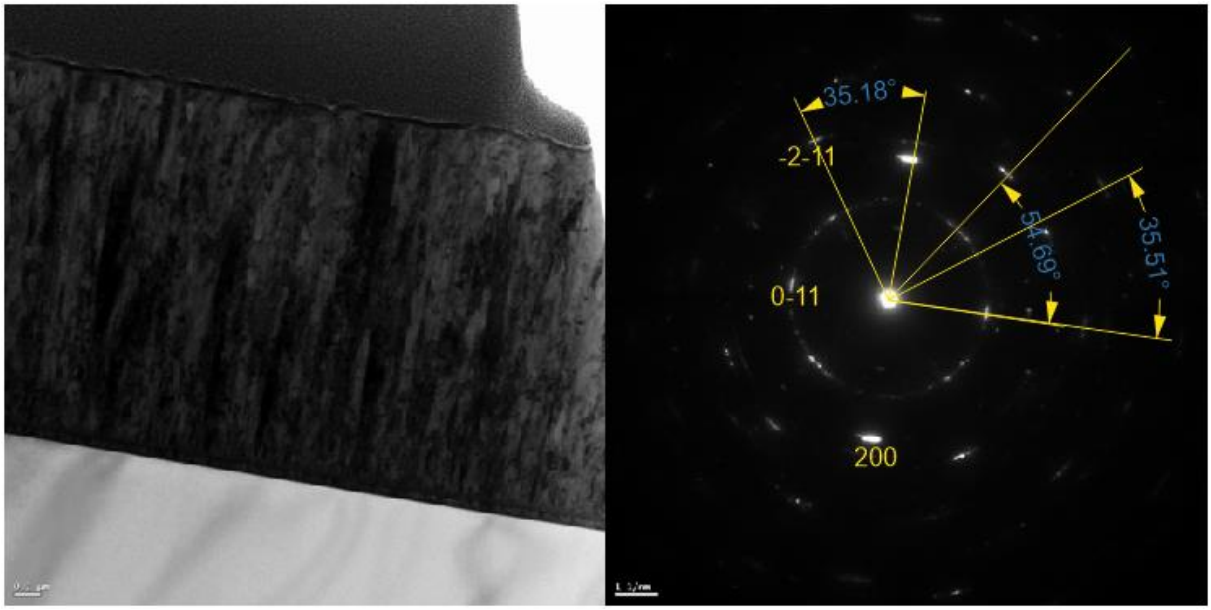

Figure 5-aa Transmission Electron Microscopy of the 5 component 5at%Nb HEA (Image of the Lamella & SAED Pattern)

Columnar grains can be visualized from the TEM lamellae. The SAED pattern alongside, depicts the presence of a BCC crystal lattice structure which also shows the texturized nature (intensity of the beam as observed) of the sample. Hence, it can be concluded from all the above experiments that the sputtered 5 component alloy is a crystalline single phase body centered cubic, elements being distributed uniformly even at nano scale; showing no phase segregation in Atom Probe Tomography. This sample is then tested for its magnetic properties.

The fact that Nb stabilizes a BCC structure for an atomic concentration ranging from around 4 to 9 at% can be explained by its difference in atomic radius with other elements. The atomic radius of Nb is larger than the other constituting elements and therefore when Nb is incorporated into a FCC lattice (quaternary FeMnCoNi), because of a higher atomic radius, it tends to stabilize a lattice which has a lower packing fraction..

5.8. MAGNETIC CHARACTERIZATION

The 5 component system so analyzed is tested for its magnetic properties. Hysteresis loops are measured at room temperature and comparisons are made between different alloy systems

or same alloy system with different compositions. The results are being discussed in this section.

Figure 5-bb shows the hysteresis loop for the alloy $Fe_{24.5}Mn_{24}Co_{23.2}Ni_{23.3}Nb_5$, inset illustrates the magnified view of this loop, to analyze the coercivity for this composition. The magnetization saturation value for this particular composition is measured to be around 174.57 emu/g and the coercivity is around 44Oe. The alloy system for this particular composition, behaves like a soft magnetic material with superior saturation magnetization value.

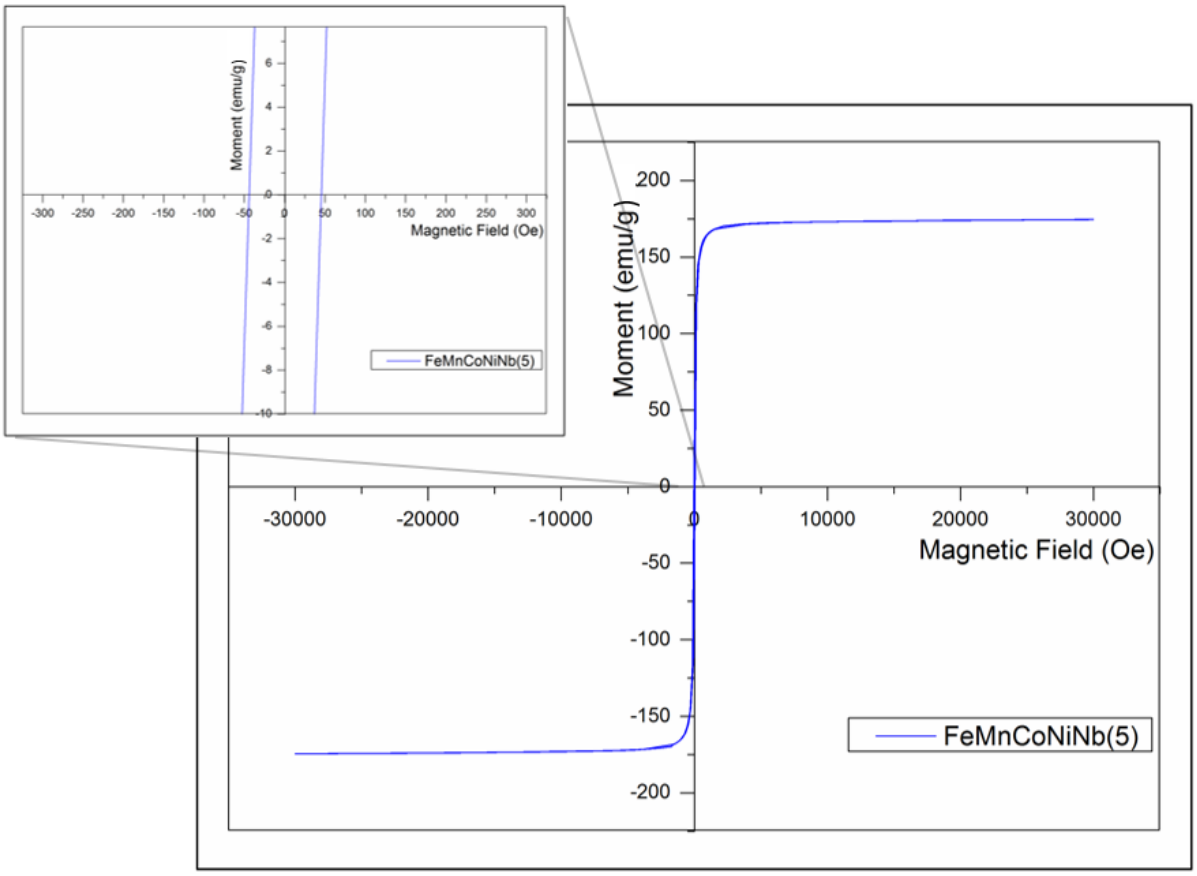

Figure 5-bb Hysteresis Loop of the 5 component alloy system $Fe_{24.5}Mn_{24}Co_{23.2}Ni_{23.3}Nb_5$

The effect of temperature variation on the magnetic properties of this sample is measured by the same VSM arrangement. The measurement is done in 2 parts- first, measuring at the lower temperature ranges from 20K to 300K at a constant magnetic field of 50 Oe; second, measuring the other temperature range from 300K to 900K at the same constant applied magnetic field.

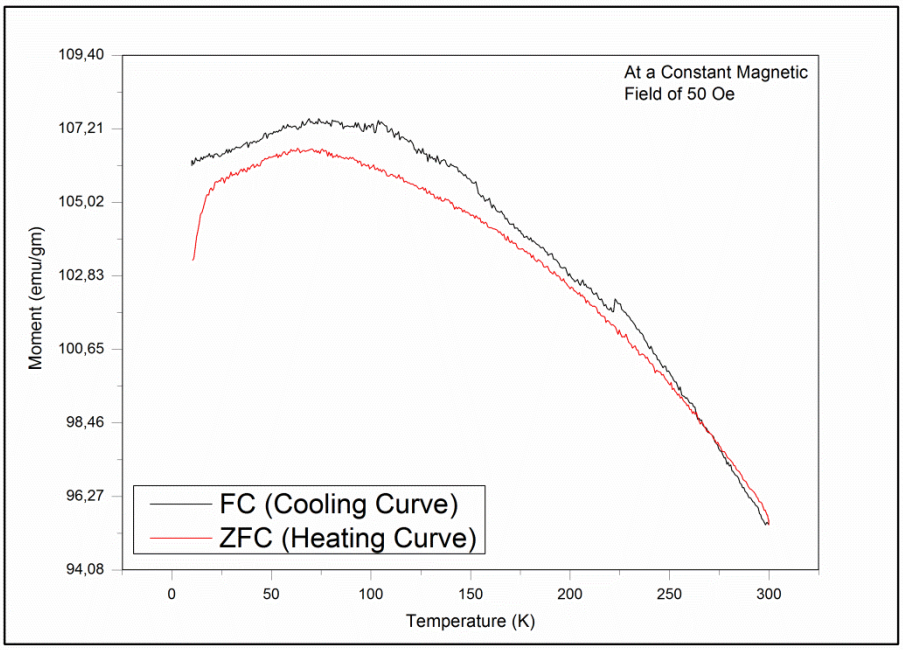

Figure 5-cc FC and ZFC curves for $Fe_{24.5}Mn_{24}Co_{23.2}Ni_{23.3}Nb_5$ 5 component alloy system.

The Figure 5-cc shows the characteristic ferromagnetic behavior for the analyzed sample. Magnetic moments acquired after magnetization, increases on lowering the temperature. There is no magnetic transformation visible in this range and hence it is of great interest to study the effect of higher temperatures on the magnetic moments.

A comparison is made between the 4 component system with equiatomic composition and the 5 component system with 5 at% Nb and the rest of elements approximately equiatomic, in order to investigate the effect of Nb and the stabilized BCC structure. The precise alloy systems measured are $Fe_{24.5}Mn_{24.5}Ni_{25.7}Co_{25.3}$ and $Fe_{24.5}Mn_{24}Ni_{23.2}Co_{23.3}Nb_5$.

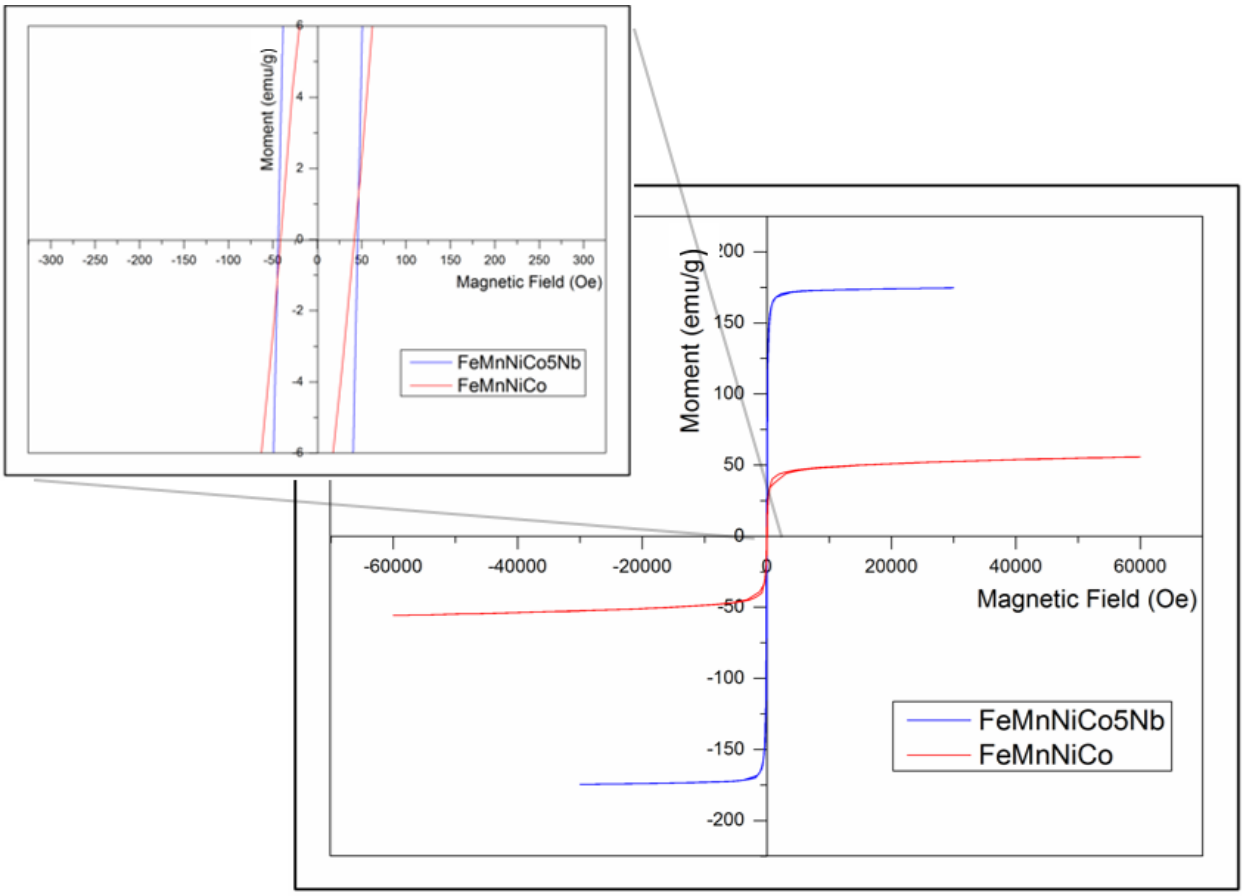

Figure 5-dd Comparison between the Hysteresis Loops of the 5 component system and the 4 component system.

The hysteresis loops illustrated in Figure 5-dd shows the superior magnetic properties of the 5 component system over the 4 component system. Even with an increase in the content of the non-magnetic element, there is a visibly higher magnetic moment attained by the 5 component system. The saturation magnetization of the 4 component system is seen to be around 54.18 emu/g in comparison to the 5 component system having the saturation magnetization value of 174.57 emu/g. The coercivity difference is not much between the 2 systems.

The higher saturation value is attributed to the BCC crystal structure stabilized over the FCC structure in the quaternary system. A BCC crystal structure preferably enhances the magnetic properties of an alloy system because of the atom placed at the body center which allows exchange spin coupling (similar to that in Heusler alloys), thus enhancing the overall magnetic moment of the system. In the section 2.4, one can notice noble properties of a BCC structure over the FCC structure, hence is the conclusion drawn here too.

These magnetic properties of the 5 component system are also compared by varying the Nb content in the alloy system. Figure 5-ee shows the hysteresis loop of both the systems - $Fe_{20.3}Mn_{17.3}Ni_{22.3}Co_{30}Nb_{10.1}$ and $Fe_{24.5}Mn_{24}Ni_{23.3}Co_{23.2}Nb_{5.}$

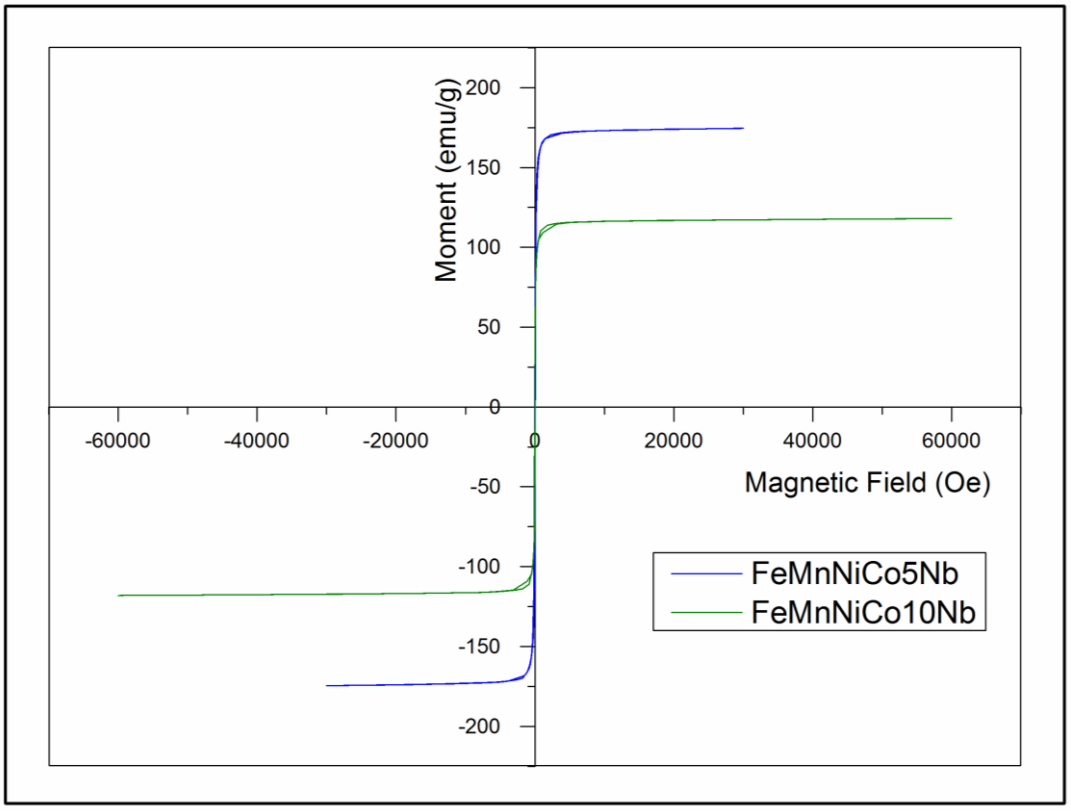

Figure 5-ee Comparison between the Hysteresis Loops of the 5 component systems, varying Nb content.

On increasing the Nb content also the magnetic properties are seen to decrease from 174.57 emu/g to around 118 emu/g (for the higher Nb containing alloy system).

Similar comparison is done with the quaternary alloy system, varying the Co content, shown in Figure 5-ff. As discussed previously, there is a visible phase separation on increasing the Co content when Mn content is above 18 at%. This same composition is compared with the equiatomic quaternary alloy system which was seen to be a single phase FCC structure. The higher Co content showing phase separation showed a higher saturation magnetization than the single FCC phase. The second phase so present might be a reason to the increased saturation of the sample.. In comparison to the 54.18 emu/g for $Fe_{24.5}Mn_{24.5}Ni_{25.7}Co_{25.3,}$ the saturation magnetization for the alloy containing 30at% Co is around 85 emu/g.

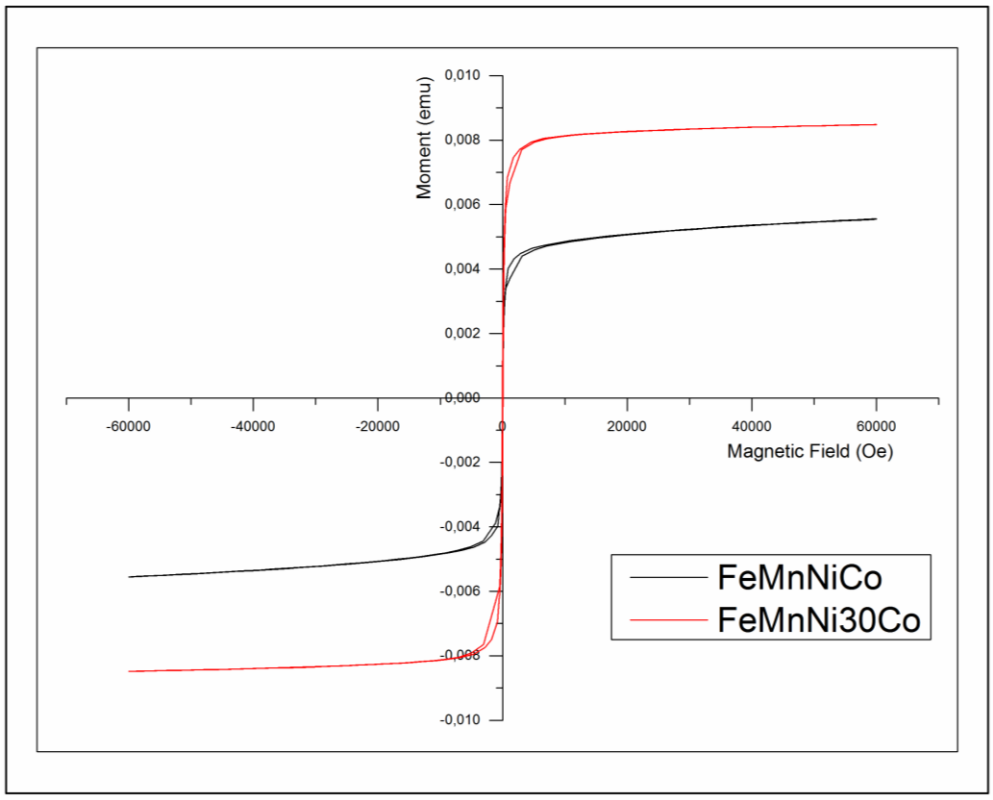

Figure 5-ff Comparison between the Hysteresis Loops of the 4 component systems, varying the Co content, showing phase separation in the already present FCC phase.

The motive of the present study has been successfully achieved by designing an alloy that has very high magnetic properties as illustrated in the given table. This alloy has properties comparable to the already known magnetic materials.

Elements/ High Entropy Alloy studied	Saturation magnetization	Phases Formed
	emu/g, Am2/Kg	
Fe	218	BCC
$Fe_{24.5}Mn_{24}Ni_{23.3}Co_{23.2}Nb_5$	~175	BCC
Co	143	HCP
FeNi	129	FCC
Ni	48,5	FCC

Table 5-2 Nobel Magnetic properties of the alloy so designed in comparison to the already existing magnetic materials.

CHAPTER 6

CONCLUSION

Using the previously discussed observations one can conclude a reasonable consideration chart for the formation of a single phase solid solution in the present alloy system i.e. FeMnNiCoNb. All the inferences from the binary, ternary, quaternary and the 5 component system are hence briefly summarized.

Alloy System	Components	Nb (at%)	Mn (at %)	Fe (at%)	Co (at%)	Ni (at%)	Phase -as formed
Binary	FeMn	-	≤ 40	Rest	-	-	BCC
		-	≥ 40	Rest	-	-	α-Mn type structure
	NiCo	-	-	-	≤ 50	Rest	FCC
		-	-	-	50≤ x ≤ 60		FCC+HCP
Ternary	FeMnNi	-	32.37 to 56.35	54.43 to 31.07	-	11.22 to 17.59	α-Mn type structure
	FeMnCo	-	34.02 to 60.03	23.3 to 59.24	5.15 to 30.59	-	α-Mn type structure
Quaternary	FeMnNiCo	-	18.01 to 25.9	22.59 to 26.15	21.75 to 27.72	26.34 to 34.64	FCC
		-	More than 18	Rest	28 to 34.02	20.64 to 26	FCC+HCP
Nb Addition	FeMnNb	7 to 33	Equiatomic		-	-	Amorphous

	FeMnNiNb	8 to 12.4	~Equiatomic		-	Rest	Amorphous
	FeMnCoNb	8 to 12	~Equiatomic		Rest	-	Amorphous
	FeMnNiCoNb	4.99 to 8.39	≥18.81	≥20.82	≥19.94	≥18.47	BCC at 300˚C
		≥9	~17.27	~20.27	~28.54	~23.96	Amorphous

The phase formation characteristics and effect of each element is understood in detail by study conducted on the alloy system FeMnNiCoNb. A single phase High Entropy Alloy has been reported and checked for its magnetic properties. Various compositions and their magnetic properties have been reported and hence the study conducted, successfully illustrates that magnetic properties of a material can be tailored significantly by a sagacious selection of the elements and their composition. This study conducted, contributes fairly towards a noble magnetic material with comparable properties to that of the other well-known ferromagnetic elements.

Elements/ High Entropy Alloy studied	**Saturation magnetization**	**Phases Formed**
	emu/g, Am2/Kg	
Fe	218	BCC
$Fe_{24.5}Mn_{24}Ni_{23.3}Co_{23.2}Nb_5$	~175	BCC
Co	143	HCP
FeNi	129	FCC
Ni	48,5	FCC
$Fe_{24.5}Mn_{24}Ni_{23.3}Co_{23.2}Nb_{10}$	~118	Amorphous
$Fe_{24,5}Mn_{24,5}Ni_{25,5}Co_{25,5}$	~54	FCC
$Fe_{24,5}Mn_{22,5}Ni_{22,7}Co_{30,3}$	~86	FCC+HCP

6.1. FUTURE WORK

The alloy designed **$Fe_{24.5}Mn_{24}Ni_{23.3}Co_{23.2}Nb_5$** with outstanding magnetic properties can be more deeply understood in terms of its atomic structure. Study of spin moments and influence of all the constituting elements in terms of magnetic properties, can be more explicitly studied.

The magnetic properties can also be probed in terms of its directional nature dependent on the grain structure and the arrangement of the magnetic domains to analyze the soft and hard direction in the alloy designed.

Other compositional gradient i.e. the Ni rich to Co rich direction of the combinatorial sample can be measured for its magnetic properties to identify change in saturation magnetization with the change in these components in order to tune this property in the favorable direction.

Application based study can be conducted i.e. electrical properties and other property characterization can be carried out in order to find its specific use in a particular area of interest.

REFERENCES

1. Pradeep, K.G., et al., *Atomic-scale compositional characterization of a nanocrystalline AlCrCuFeNiZn high-entropy alloy using atom probe tomography.* Acta Materialia, 2013. **61**(12): p. 4696-4706.
2. Zhang, Y., et al., *Microstructures and properties of high-entropy alloys.* Progress in Materials Science, 2014. **61**: p. 1-93.
3. Yao, M.J., et al., *A novel, single phase, non-equiatomic FeMnNiCoCr high-entropy alloy with exceptional phase stability and tensile ductility.* Scripta Materialia, 2014. **72–73**: p. 5-8.
4. Otto, F., et al., *The influences of temperature and microstructure on the tensile properties of a CoCrFeMnNi high-entropy alloy.* Acta Materialia, 2013. **61**(15): p. 5743-5755.
5. Deng, Y., et al., *Design of a twinning-induced plasticity high entropy alloy.* Acta Materialia, 2015. **94**: p. 124-133.
6. Porter, D.A. and K.E. Easterling, *Phase transformations in metals and alloys*. 1992: Chapman & Hall.
7. Takeuchi, A., et al., *Alloy Design for High-Entropy Bulk Glassy Alloys.* Procedia Engineering, 2012. **36**: p. 226-234.
8. Zhang, Y., et al., *Solid-Solution Phase Formation Rules for Multi-component Alloys.* Advanced Engineering Materials, 2008. **10**(6): p. 534-538.
9. Guo, S., et al., *Effect of valence electron concentration on stability of fcc or bcc phase in high entropy alloys.* Journal of Applied Physics, 2011. **109**(10): p. 103505.
10. Murty, B.S., J.W. Yeh, and S. Ranganathan, *Chapter 1 - A Brief History of Alloys and the Birth of High-Entropy Alloys*, in *High Entropy Alloys*. 2014, Butterworth-Heinemann: Boston. p. 1-12.
11. Murty, B.S., J.W. Yeh, and S. Ranganathan, *Chapter 2 - High-Entropy Alloys: Basic Concepts*, in *High Entropy Alloys*. 2014, Butterworth-Heinemann: Boston. p. 13-35.
12. Kao, Y.-F., Chen S-K., Chen T-J., Chu P-C., Yeh J-W., Lin S-J., *Electrical, magnetic, and Hall properties of AlxCoCrFeNi high-entropy alloys.* Journal of Alloys and Compounds, 2011. **509**(5): p. 1607-1614.
13. Liu, L., Zhu J.B., Li J.C., Jiang Q., *Microstructure and Magnetic Properties of FeNiCuMnTiSnx High Entropy Alloys.* Advanced Engineering Materials, 2012. **14**(10): p. 919-922.
14. Lucas, M.S., Belyea D., Bauer C., Bryant N., Michel E., Turgut Z., *Thermomagnetic analysis of FeCoCrxNi alloys: Magnetic entropy of high-entropy alloys.* Journal of Applied Physics, 2013. **113**(17): p. 17A923.
15. Lucas, M.S., Mauger L., Munoz J.A., Xiao Y., Sheets A.O., Semiatin S.L., Horwath J., Turgut Z., *Magnetic and vibrational properties of high-entropy alloys.* Journal of Applied Physics, 2011. **109**(7): p. 07E307.

16. Körmann, F., Ma D., Belyea D.D., Lucas M.S., Miller C.W., Grabowski B., Sluiter M.H.F., *"Treasure maps" for magnetic high-entropy-alloys from theory and experiment.* Applied Physics Letters, 2015. **107**(14): p. 142404.

17. Ma, S.G. and Y. Zhang, *Effect of Nb addition on the microstructure and properties of AlCoCrFeNi high-entropy alloy.* Materials Science and Engineering: A, 2012. **532**: p. 480-486.

18. Zhang, K.B., Fu Z.Y., Shi J., Wang W.M., Wang H., Wang Y.C., Zhang Q.J., *Annealing on the structure and properties evolution of the CoCrFeNiCuAl high-entropy alloy.* Journal of Alloys and Compounds, 2010. **502**(2): p. 295-299.

19. Singh, S., Wanderka N., Keifer K., Siemensmeyer K., Banhart J., *Effect of decomposition of the Cr–Fe–Co rich phase of AlCoCrCuFeNi high entropy alloy on magnetic properties.* Ultramicroscopy, 2011. **111**(6): p. 619-622.

20. Wang, Y.P., B.S. Li, and H.Z. Fu, *Solid Solution or Intermetallics in a High-Entropy Alloy.* Advanced Engineering Materials, 2009. **11**(8): p. 641-644.

21. Wang, X.F., Zhang Y., Qiao Y., Chen G.L., *Novel microstructure and properties of multicomponent CoCrCuFeNiTix alloys.* Intermetallics, 2007. **15**(3): p. 357-362.

22. Zhang, H., Pan Y. He Y., Jiao H., *Microstructure and properties of 6FeNiCoSiCrAlTi high-entropy alloy coating prepared by laser cladding.* Applied Surface Science, 2011. **257**(6): p. 2259-2263.

23. Tariq, N.H., Naeem M., Hasan B.A., Akhter J., Siddique M., *Effect of W and Zr on structural, thermal and magnetic properties of AlCoCrCuFeNi high entropy alloy.* Journal of Alloys and Compounds, 2013. **556**: p. 79-85.

24. Wang, J., Zheng Z., Xu J., Wang Y., *Microstructure and magnetic properties of mechanically alloyed FeSiBAlNi (Nb) high entropy alloys.* Journal of Magnetism and Magnetic Materials, 2014. **355**: p. 58-64.

25. Yao, C.-Z., Zhang P., Meng L., Li G-R., Ye J-Q., *Electrochemical preparation and magnetic study of Bi–Fe–Co–Ni–Mn high entropy alloy.* Electrochimica Acta, 2008. **53**(28): p. 8359-8365.

26. Zhang, Y., Zuo T.T., Cheng Y-Q., Liaw P.K., *High-entropy Alloys with High Saturation Magnetization, Electrical Resistivity, and Malleability.* Scientific Reports, 2013. **3**: p. 1455.

27. Zuo, T., Yang X., Liaw P K., Zhang Y., *Influence of Bridgman solidification on microstructures and magnetic behaviors of a non-equiatomic FeCoNiAlSi high-entropy alloy.* Intermetallics, 2015. **67**: p. 171-176.

28. Chen, C.-W., *Magnetism and Metallurgy of Soft Magnetic Materials.*

29. Takeuchi, A. and A. Inoue, *Classification of Bulk Metallic Glasses by Atomic Size Difference, Heat of Mixing and Period of Constituent Elements and Its Application to Characterization of the Main Alloying Element.* MATERIALS TRANSACTIONS, 2005. **46**(12): p. 2817-2829.

30. Guo, S. and C.T. Liu, *Phase stability in high entropy alloys: Formation of solid-solution phase or amorphous phase.* Progress in Natural Science: Materials International, 2011. **21**(6): p. 433-446.

31. www.wikipedia.org.

32. B.C., D., *Magnetic Media, Measurements with a VSM.* Lake Share Cryotronics, Inc www.lakeshore.com.

33. Committees, A.I.A.P.D.a.t.H., *Alloy Phase Diagrams.* ASM Handbook, 1992. **3**.

34. Proult, A. and P. Donnadieu, *A simple description of the α-manganese (A12) structure derived from defect studies.* Philosophical Magazine Letters, 1995. **72**(5): p. 337-344.

35. Inoue, A., *Stabilization of metallic supercooled liquid and bulk amorphous alloys.* Acta Materialia, 2000. **48**(1): p. 279-306.